american physiological society
AMERICAN JOURNAL OF PHYSIOLOGY
CELL PHYSIOLOGY

Am J Physiol Cell Physiol 328: C335–C354, 2025.
First published December 14, 2024; doi:10.1152/ajpcell.00669.2024

RESEARCH ARTICLE

Sulforaphane treatment mimics contractile activity-induced mitochondrial adaptations in muscle myotubes

Sabrina Champsi and David A. Hood

Muscle Health Research Centre, School of Kinesiology and Health Science, York University, Toronto, Ontario, Canada

Abstract

Mitochondria are metabolic hubs that govern skeletal muscle health. Although exercise has been established as a powerful inducer of quality control processes that ultimately enhance mitochondrial function, there are currently limited pharmaceutical interventions available that emulate exercise-induced mitochondrial adaptations. To investigate a novel candidate for this role, we examined sulforaphane (SFN), a naturally occurring compound found in cruciferous vegetables. SFN has been documented as a potent antioxidant inducer through its activation of the nuclear factor erythroid 2-related factor 2 (Nrf-2) antioxidant response pathway. However, its effects on muscle health have been underexplored. To investigate the interplay between chronic exercise and SFN, C2C12 myotubes were electrically stimulated to model chronic contractile activity (CCA) in the presence or absence of SFN. SFN promoted Nrf-2 nuclear translocation, enhanced mitochondrial respiration, and upregulated key antioxidant proteins including catalase and glutathione reductase. These adaptations were accompanied by reductions in cellular and mitochondrial reactive oxygen species (ROS) emission. Signaling toward biogenesis was enhanced, demonstrated by increases in mitochondrial transcription factor A (TFAM), peroxisome proliferator-activated receptor-gamma coactivator (PGC)-1α nuclear translocation, PGC-1α promoter activity, mitochondrial content, and organelle branching, suggestive of a larger, more interconnected mitochondrial pool. These mitochondrial adaptations were accompanied by an increase in lysosomal proteins, suggesting coordinated regulation. There was no difference in mitochondrial and antioxidant-related proteins between CCA and non-CCA SFN-treated cells. Our data suggest that SFN activates signaling cascades that are common to those produced by contractile activity, indicating that SFN-centered therapeutic strategies may improve the mitochondrial phenotype in skeletal muscle.

NEW & NOTEWORTHY Nrf-2 is a transcription factor that has been implicated in mitigating oxidative stress and regulating mitochondrial homeostasis. However, limited research has demonstrated how Nrf-2-mediated adaptations compare with those produced by exercise. To investigate this, we treated myotubes with Sulforaphane, a well-established Nrf-2 activator, and combined this with stimulation-induced chronic contractile activity to model exercise training. Our work is the first to establish that sulforaphane mimics training-induced mitochondrial adaptations, including enhancements in respiration, biogenesis, and dynamics.

exercise; mitochondrial biogenesis; Nrf-2; PGC-1α; skeletal muscle

INTRODUCTION

Skeletal muscle health is heavily influenced by the quantity and quality of the mitochondria that reside within it. Loss of mitochondria and excessive reactive oxygen species (ROS) emission have both been linked to muscle atrophy, indicating that mitochondria are tightly linked to muscle health (1, 2). Mitochondria are exceedingly adaptable and are capable of modulating their structure and molecular response to fulfill the tissue's energy demand (3, 4). The plasticity of this organelle is exemplified during exercise, where several intracellular signaling cascades are activated, which ultimately drive mitochondrial quality control processes, such as biogenesis (5).

Due to the presence of both nuclear and mitochondrial-DNA encoded proteins, coordination of both genomes is required to mediate this process (6, 7). The most prominent regulator of biogenesis within the literature is peroxisome proliferator-activated receptor-gamma coactivator-1α (PGC-1α) (8–12). PGC-1α mediates biogenesis by coactivating transcription factors involved in the upregulation of nuclear genes encoding mitochondrial proteins (13, 14). However, the coregulatory role of this protein is only activated upon a series of posttranslational modifications (5). Specifically, acute exercise enhances the activation of Ca^{2+}/calmodulin-dependent protein kinase (CaMK) (15), p38 mitogen-activated protein kinase (MAPK) (16, 17), and AMP-kinase (AMPK) (18, 19), which all subsequently phosphorylate PGC-1α and permit its nuclear translocation (20). Within the nucleus, PGC-1α coactivates nuclear respiratory factor 1 (NRF-1), a transcription factor involved in the expression of mitochondrial transcription factor A (TFAM), the most important mediator of mitochondrial DNA transcription and replication (21, 22).

In addition to the synthesis of new mitochondria, it is essential that poorly functioning and damaged mitochondria

Correspondence: D. A. Hood (dhood@yorku.ca).
Submitted 12 September 2024 / Revised 15 November 2024 / Accepted 3 December 2024

are removed and broken down through lysosomal-mediated mechanisms (23). This ensures that the quality of the mitochondrial pool is maintained or improved, preserving cellular function (24). Chronic exercise has been reported to enhance the capacity for mitochondrial removal through lysosomal biogenesis, thereby better equipping the cell for mitochondrial turnover (24–26). A major regulator of this process is transcription factor E3 (TFE3), which enhances the expression of lysosomal and autophagy-related genes (27).

Training has also been reported to reduce ROS through the upregulation of antioxidant proteins, such as glutathione peroxidase-1 (28, 29) and glutathione reductase (29, 30). Central to this axis, and mediator of these targets, is the transcription factor nuclear factor erythroid 2-related factor 2 (Nrf-2) (31). Under basal conditions, Nrf-2 is sequestered within the cytosol by its negative regulator Kelch-likeenoyl-coA hydratase (ECH)-associated protein 1 (Keap1) (32). Keap1 acts as an adaptor for the E3 ubiquitin ligase complex cullin 3 (Cul3), permitting the ubiquitination and degradation of Nrf-2, thus keeping protein levels extremely low (32). During exercise, ROS modify sensitive cysteine residues on Keap1, resulting in a reduction in Nrf-2 ubiquitination (33). Nrf-2 is then able to accumulate, translocate to the nucleus, and heterodimerize with members of the small Musculo-aponeurotic fibrosarcoma protein family, permitting its binding to antioxidant response elements (ARE) found upstream of target genes (34). Although this signaling cascade has been reported to occur during exercise (35), it can be chemically induced by the nutraceutical sulforaphane (SFN) (36). SFN has proven to be an extremely strong inducer of the Nrf-2-Keap1 axis and therefore has been used in several studies to examine the downstream effectors of this pathway (37–39).

SFN is a naturally occurring compound found in cruciferous vegetables, such as broccoli and cauliflower (38, 40). Although previous work has positioned SFN as a chemopreventive agent (41), recent work has revealed that it may play an important role in mitochondrial homeostasis. The most convincing evidence is that Nrf-2 enhances the transcription of NRF-1, which drives TFAM expression and mitochondrial DNA copy number (42). Conversely, knockdown of Nrf-2 within skeletal muscle has been shown to reduce mitochondrial respiration, increase mitochondrial ROS emission, and increase muscle fatigability (43), suggesting that Nrf-2 has a direct influence on muscle health. Since SFN has been described as among one of the most potent Nrf-2 activators available, we chose to investigate the effects of SFN in C2C12 myotubes to elucidate if *1*) Nrf-2 may be able to preserve or enhance the mitochondrial content and function and if *2*) sustained Nrf-2 activation may augment mitochondrial adaptations in response to exercise using an in vitro model of CCA.

METHODS

Growth, Maintenance, and Differentiation of C2C12 Murine Skeletal Muscle Cells

C2C12 myoblasts (ATCC Catalog No.: CRL-1772; RRID: CVCL_0188), an established cell line, were grown in Dulbecco's modified Eagle's medium (DMEM; Wisent), supplemented with 10% fetal bovine serum (FBS; Fisher) and 1% penicillin-streptomycin (P/S; Wisent) [growth medium (GM)]. Cells were incubated at 37°C and 5% CO_2 and passaged upon 60% confluency to maintain their myoblast form. For subsequent treatment and analysis of SFN on myotubes, C2C12 myoblasts are seeded in 6-well cell culture plates supplemented with GM. After reaching 80–90% confluency, GM was removed and cells were washed with PBS before incubation with differentiation media (DM), containing 5% heat-inactivated horse serum and 1% P/S to promote differentiation. DM was replaced daily to promote cell health and differentiation. After 6 days of differentiation, myotube morphology was confirmed using a phase contrast microscope before performing subsequent treatment and analysis. All experiments were completed on myotubes between passages 10 and 15.

Drug Treatments

A 10 mM stock solution of SFN (MedChemExpress) was prepared using DMSO (Sigma) as the diluent. An intermediate stock of 2 mM was further produced using DMSO, and a final working concentration of 10μM was obtained by adding a portion of the 2 mM stock directly to DM and finally added directly to the cells. Vehicle treatment was prepared by adding the same volume of DMSO to DM. The proteasome inhibitor *N*-carbobenzoxyl-Leu-Leu-leucinal (MG132; Sigma) was prepared as a 2 mM stock solution and was added to SFN or vehicle-treated media to produce a final working concentration of 10μM. Cells were cotreated with SFN and MG132 for 6 h in phenol-free media before imaging. Positive and negative controls for flow cytometry were prepared fresh and performed every time a new vial of dye was used. The antioxidant *N*-acetylcysteine (NAC; Sigma) was used as a negative control for CellROX Green, as this agent reduces all ROS permitting no CellROX Green signal. A 100 mM stock solution of NAC was prepared using DMSO, and a final working concentration of 20 mM was used to treat myotubes for 24 h (18). The ROS inducer menadione (Sigma) (44) was used as a positive control for CellROX Green. A 50 mM stock of Menadione was prepared by resuspending the powder in DMSO, prior to producing the final working concentration of 100μM and treating for 1 h, as per the manufacturer's instructions. For mitochondrial ROS (mtROS) experiments using MitoSOX Red, Rotenone, an inhibitor of complex 1 of the electron transport chain was used. Inhibition of this complex induces excessive mtROS emission, therefore serving as a positive control for MitoSOX Red fluorescence. Rotenone was prepared as a 1 mM stock solution and finally prepared as a 200 nM working concentration. To assess the efficacy of MitoTracker Red (MTR), a detector of mitochondrial membrane potential, the mitochondrial uncoupler carbonyl cyanide m-chlorophenylhydrazone (CCCP; Sigma) was used. CCCP acts to dissipate membrane potential, thus ensuring no MTR signal and serving as a negative control. A 100 mM stock solution of CCCP was prepared, and finally a working concentration of 25μM was produced and applied to cells for 30 min before flow experiments (45).

Whole Cell Isolation and Protein Extraction

Following treatment, media was aspirated, and cells were rinsed twice with warm PBS. Cells were then trypsinized for 5 min at 37°C to permit cell detachment before being scraped, collected, and spun down at 1,400 *g* for 4 min.

Following centrifugation, the supernatant fraction was aspirated, and the pellet was resuspended in ice-cold PBS. Cells were spun down again at 1,400 *g* for 4 min and PBS was aspirated. The pellet was placed on ice and resuspended in cell extraction buffer containing 1X lysis buffer (Promega), phosphatase inhibitor cocktails (Sigma), and a protease inhibitor (Sigma). Four freeze-thaw cycles were performed by flash-freezing cells with liquid nitrogen then thawing them in a 37°C water bath. This procedure damages the cell membrane and promotes cell lysis. Finally, cell lysates were centrifuged at 2,500 *g* for 10 min at 4°C and the supernatant fraction was collected and stored in −80°C for future use.

Nuclear-Cytoplasmic Fractionation

C2C12 myoblasts were seeded and differentiated in 15 cm^2 cell culture plates before treatment with SFN or vehicle. Whole cells were collected in cytoplasmic buffer, containing phosphatase inhibitor cocktails (Sigma), and a protease inhibitor (Sigma). Samples were placed on ice for 5 min before being rocked on the orbital shaker for 5 min at 4°C, then centrifuged at 2,500 *g* for 4 min. The supernatant fraction was collected and stored as the cytoplasmic fraction at −80°C for future use. The remaining nuclear fraction was resuspended with cytoplasmic buffer, rocked for 3 min at 4°C, and then centrifuged at 3,200 *g* for 4 min before discarding the supernatant fraction. This workflow was repeated 10–12 times to ensure the purity of the nuclear fraction. After the final cycle, 0.15 unit/μL of Benzonase (Sigma) was added to the nuclear fraction and incubated on ice for 20 min before storing the samples at −80°C for subsequent Western blotting.

Western Blotting

The protein concentration of each sample was determined using the Bradford assay. Equal amounts of protein, ranging from 15 to 30 μg depending on the protein targets, were prepared for Western blotting. Briefly, equal amounts of crude protein from whole cell extractions were combined with Laemmli sample buffer. Laemmili buffer was prepared by combining 9.375 mL 1 M Tris (pH = 6.8), 1.5 g SDS, and 1.2 mL glycerol. This solution was mixed until fully homogenous at 40°C, prior to adding 2.25 mL β-mercaptoethanol and 7.5 mg Bromophenol Blue and topping up to 25 mL with ddH_2O. Laemmili buffer was aliquoted and stored at −20°C until ready to use. Samples were denatured at 95°C for 7 min and topped up with cell extraction buffer. Samples were loaded into 8–15% sodium dodecyl sulfate (SDS) polyacrylamide gels and separated using electrophoresis. Following separation, proteins were transferred onto nitrocellulose membranes and washed with Ponceau S stain (Sigma) to confirm that transferring was successful. Membranes were labeled and cut at the appropriate molecular weight for each target protein. Ponceau S stain was washed off the membranes with 1X TBS-T for 5 min before blocking for 1 h in 5% skim milk at room temperature with light agitation. Afterward, primary antibodies (see Table 1) were applied to membranes overnight at 4°C. The following day, membranes were incubated with the corresponding secondary antibody for 1 h at room temperature. Equal portions of Clarity Max Enhanced Chemiluminescence (ECL; BioRad) substrates were combined and applied to membranes for 4 min before being imaged using the iBright Imaging System (Thermo Fisher). Optical density was quantified using ImageJ software (ver. 1.53) for subsequent quantification using GraphPad Prism Software (ver. 8.2.1). All protein targets, apart from nuclear-cytosolic fractions, were normalized to their corresponding GAPDH following imaging. Due to the similar molecular weights of target proteins, membranes were stripped and reprobed with the appropriate primary antibody in the presence of sodium azide to avoid cutting blots too closely. This process removes any horseradish peroxidase (HRP) from the secondary antibody. Stripping was only completed on blots with different secondaries to avoid residual signals from the previous target. Western blotting for nuclear and cytosolic fractions was normalized to Ponceau, given that Histone 2B (H2B) did not fit on the gel percentage for each target. H2B and α-tubulin were used to demonstrate fraction purity. It should be noted that Cathepsin B exhibits two bands, a smaller band depicting the cleaved, mature protease, and a larger band demonstrating the premature, non-cleaved band. As there is more mature Cathepsin B protein relative to premature, a long exposure is required to visualize the premature band, rendering the mature band overexposed as shown in red (Fig. 7).

Flow Cytometry

Myoblasts were proliferated and differentiated in a 6-well cell culture plate, before treatment with SFN and vehicle. Cells were stained with 100 nM MitoTracker Green (MTG; Fisher), 100 nM MitoTracker Red (MTR; Fisher) 5 mM CellROX Green (Fisher), or 15 μM MitoSOX Red (Fisher) in phenol-free media (Life Tech) for 30 min at 37°C. Following incubation, myotubes were washed with warm PBS, trypsinized for 5 min at 37°C, and then scraped for collection and centrifugation at 1,400 *g* for 4 min. Pellets were washed and then resuspended in roughly 250 μL of ice-cold PBS before being analyzed on the Flow Cytometer (Beckman, CytoFlex). Resuspension of cells in a large volume of PBS was performed to avoid clogging of the cytometer's tubing system. MTG and CellROX Green were evaluated using the fluorescein isothiocyanate (FITC) filter, while MTR and MitoSOX Red were assessed using the phycoerythrin (PE) filter, both using the 488 nm laser. Unstained, single stains, and double-stained samples were produced for each experiment to generate accurate gating for dot plots. Compensation was performed when applying more than one dye to correct for spectral overlap, thereby providing a more accurate fluorescence intensity for each dye (Supplemental Fig. S1). For each biological replicate, three technical replicates were produced, and the fluorescent reading was averaged upon reading on the flow cytometer. For each technical replicate, 40,000 events were recorded to ensure that the same number of cells were evaluated for each condition. To avoid clogging and accurate fluorescent readings, the sample flow rate was not permitted to exceed 3,000 events/s, ensuring the sample volume did not exceed 10uL. Daily quality control (QC) was performed before every experiment to confirm that the instrument was working correctly and providing adequate signal strength and provision. Briefly, a small aliquot of the CytoFlex ready-to-use QC fluorospheres (Beckman; C65719) was added to an Eppendorf tube, vortexed, and subjected to a QC experiment. Results are expressed as mean peak fluorescence intensity.

Table 1. *List of antibodies used for Western blotting*

Antibody	Manufacturer	Catalog No.	Molecular Weight, kDa	[1°Ab]	[2°Ab]
Nrf-2	Cell Signaling	12721S	100	1:500	1:1,000
P62 (SQSTM1)	Cell Signaling	5114S	62	1:1,000	1:1,000
Keap1	ProteinTech	10503-2-AP	74	1:1,000	1:2,000
H2B	Cell Signaling	2934S	15	1:1,000	1:1,000
α-tubulin	Millipore Sigma	CP06- 100UG	50	1:1,000	1:1,000
GAPDH	Abcam	ab9485	37	1:100,000	1:5,000
TFAM	Abcam	ab176558	24	1:500	1:1,000
COX I	Abcam	ab14705	39	1:500	1:1,000
MFN2	Abcam	ab50843	86	1:1,000	1:1,000
Glutathione Reductase	Santa Cruz	sc-133245	55	1:2,000	1:1,000
G6PD	Cell Signaling	8866S	58	1:1,000	1:1,000
NQO1	Abcam	ab34173	31	1:1,000	1:1,000
Catalase	Cell Signaling	14097S	60	1:2,000	1:1,000
GPX-1	Abcam	Ab22604	22–24	1:1,000	1:1,000
SP1	Santa Cruz	SC-420	92	1:1,250	1:1,000
CREB1	Santa Cruz	SC-058	43	1:1,000	1:1,000
ATF-2	Cell Signaling	20F1	65–75	1:1,250	1:1,000
USF-1	Santa Cruz	sc-8983	44	1:1,000	1:1,000
TFE3	Sigma	HPA023881	73	1:500	1:1,000
UQCRC2	Abcam	ab14745	48	1:1,000	1:1,000
VDAC	Abcam	ab14734	33	1:500	1:1,000
vATPase	Santa Cruz	sc-55544	50	1:1,000	1:1,000
Cathepsin B	Cell Signaling	31718S	24–44	1:1,000	1:1,000
HO-1	Abcam	ab13248	32	1:1,000	1:1,000
Drp-1	BD BioSciences	611738	27	1:1,000	1:1,000
P-AMPK (Thr172)	Cell Signaling	2535S	64	1:1,000	1:1,000
AMPK	Cell Signaling	2532S	64	1:1,000	1:1,000
P-JNK (Thr183, Tyr185)	Cell Signaling	4668S	37–54	1:1,000	1:1,000
T-JNK	Cell Signaling	9252T	37–54	1:1,000	1:1,000
P-P38 MAPK (Thr180/Tyr182)	Cell Signaling	9211S	43	1:1,000	1:1,000
P38 MAPK	Cell Signaling	9212S	40	1:1,000	1:1,000
P-CAMKII-α (Thr286)	Cell Signaling	3361S	50	1:1,000	1:1,000
T-CAMKII-α	Cell Signaling	3362S	50–60	1:1,000	1:1,000
P-GSK-3B	Cell Signaling	9322S	46	1:1,000	1:1,000
T-GSK-3B	Cell Signaling	9832S	46	1:1,000	1:1,000
Anti-Mouse HRP-linked 2°	Cell Signaling	7076S			
Anti-Rabbit HRP-linked 2°	Cell Signaling	7074S			

H2B, Histone 2B; Nrf-2, nuclear factor erythroid 2-related factor 2; TFAM, mitochondrial transcription factor A.

Assessment of Mitochondrial Content, Morphology, and PGC-1α via Confocal Microscopy

Following either SFN alone, MG132 treatment, or CCA, C2C12 myotubes were stained as described above with 10 μM Hoechst (Fisher), and either MTG or MTR in phenol-free DMEM immediately before imaging. Myotubes were imaged with the confocal microscope using a Nikon Eclipse TE2000-U Fluorescence microscope coupled to a Nikon C2 microscope. All image analysis was performed using ImageJ (ver. 1.53), ensuring fully visible myotubes were traced (i.e., minimum 2 nuclei per cell). To measure dye intensity, images were processed using "unsharp mask" (radius = 1.0 pixel, mask = 0.60) and "median" (radius = 2.0 pixels) filter tools. Images were made "binary" and "skeletonized" before measuring the integrated density (fluorescence intensity) of each channel. To assess the colocalization of MTG and MTR or Hoechst and GFP, the plugin JACop (https://github.com/fabricecordelieres/IJ-Plugin_JACoP) was used (46). Costes' automatic threshold was used to determine Mander's coefficient for each overlapping fraction. To assess mitochondrial morphology, the Mitochondria Analyzer Toolset, available as a plugin on ImageJ (https://github.com/AhsenChaudhry/Mitochondria-Analyzer), was used according to the provided user manual (47, 48). Briefly, following imaging of the mitochondrial network via MTR staining, images were obtained and plugged into ImageJ. Images were processed as described above within the methods for dye intensity, made "binary" and "skeletonized" before being imported into the Mitochondria Analyzer software. Three images were analyzed for each n ($n = 5$), ensuring that at least two myotubes were fully visible for each image. The Analyzer menu was opened and a two-dimensional (2-D) analysis was completed for each image, ensuring that various networking analyses were completed on the 2-D stack. Analysis was completed on a per-mitochondria basis, displaying results such as branch length and the number of branch junctions per mitochondria. Branch length refers to how long the mitochondrial branches are, whereas branch junction refers to points in the reticulum where two or more branches meet. Both length and intersectionality are parameters indicative of mitochondrial connectivity, therefore providing meaningful and relevant information about shifts in mitochondrial populations from fragmented to more reticular-like formation.

Mitochondrial Respiration

Mitochondrial respirometry was assessed using the Seahorse XF96 Cell Mito Stress Test Kit (Agilent). Myoblasts were seeded at a density of 2,500 cells per well and subsequently differentiated in a Seahorse cell microculture plate

(Agilent) before treatment with SFN and vehicle for 24 h and 48 h. Each condition was plated in 23 replicate wells across the microplate and averaged for each condition ($n = 1$). This experiment was completed five times on separate plates ($n = 5$). The Seahorse assay offers real-time analysis of oxygen consumption rate (OCR) following the addition of various electron transport chain inhibitors to extract various respirometry parameters in vitro. First, the XF96 Extracellular Flux Cartridge was used to measure OCR during basal respiration, followed by ATP-linked respiration after adding oligomycin, an inhibitor of ATP synthase. Subsequently, carbonyl cyanide-p-trifluoromethoxyphenylhydrazone (FCCP) was added to induced membrane uncoupling and evaluated maximal uncoupled respiration. Finally, rotenone and antimycin A, inhibitors of complexes one and three respectively, were added to measure spare respiratory capacity. After the assay was completed, cells were washed with phenol-free DMEM (Wisent; 319-065-CL) supplemented with glucose and glutamine, then incubated with 10 μM Hoechst (Thermo; 33342) and 100 nM MitoTracker Green (Thermo) for 30 min at 37°C to stain nuclei and mitochondria, respectively. Following incubation, fluorescence was measured on the BioTek Cytation 5 plate reader. MitoTracker Green was normalized to Hoechst to obtain a measurement of mitochondria per cell. These values were used to normalize the OCR obtained per well to nuclei and mitochondrial content, to better represent mitochondrial respiration per cell. This workflow was completed using the XF Wave Software (Agilent), measuring the area under the curve for each respiration parameter.

Chronic Contractile Activity

Following differentiation and confirmation of appropriate morphology, myotubes were electrically stimulated, as previously described (10, 49, 50). Briefly, the plastic lids corresponding to 6-well cell plates were retrofitted with two platinum electrodes that span the length of the well. Before stimulation, cells were washed and supplemented with 4.5 mL of fresh media per well, ensuring each electrode was fully submerged. Myotubes were subjected to electrical pulse stimulation (EPS) at 5 Hz and 18 V for 3 h, followed by a 21-h recovery period where cells were supplemented with either vehicle or SFN. Visual confirmation of myotube contraction was confirmed for every bout and monitored periodically to ensure that sustained contraction was achieved (Supplemental Video S1). Stimulation was repeated for 4 days, and cells were collected for analysis after the last recovery period (Fig. 7*A*).

Acute Contractile Activity

Myotubes were subjected to the same contractile model as described above; however, only underwent a single bout of EPS which lasted 3 h, to model acute contractile activity (ACA). Cells were collected immediately following stimulation and were treated with either SFN or vehicle during the bout. Unstimulated cells were treated for 3 h and collected at the same time as the cells subjected to contractile activity.

Promoter-Reporter Transient Transfections

A custom PGC-1α promoter-firefly-luciferase-reporter construct was purchased from Applied Biological Materials, Inc. (Richmond, BC, Canada), containing 4 kb of the mouse PGC-1α promoter region. For DNA amplification, the plasmid was transformed into competent *Escherichia coli* cells, which were incubated on ice for 30 min. Following incubation, cells were heat-shocked for 30 s and then placed back on ice for 5 min before adding 475 μL of outgrowth media (New England) and placed on a shaker plate at 37°C and 250 rpm for 1 h. Cells were inoculated on agar plates supplemented with the corresponding antibiotic (Kanamycin or Ampicillin). Following overnight incubation, single colonies were selected and amplified in luria broth (LB) media overnight on the shaker (250 rpm), followed by plasmid isolation using the HiSpeed Plasmid Maxi Prep Kit (Qiagen). The following day, 2.0 μg DNA/well of PGC-1α plasmid was cotransfected with a 0.05 μg DNA/well cytomegalovirus (CMV)-promoter-pRL3-reporter vector (Promega), expressing renilla luciferase, which served as a control for transfection efficiency. Similarly, 2.0 μg DNA/well of empty vector (EV; Promega), matching the PGC-1α plasmid, was cotransfected with 0.05 μg DNA/well of pRL3 vector to provide a baseline of luciferase activity, accounting for any nonspecific activity, which contributes to the background signal. At 40% confluency, cells were transfected with the plasmids and Lipofectamine2000 (Fisher) in serum-free DMEM. Following 17 h of transfection, myoblasts were washed with PBS, proliferated, differentiated, and treated with SFN or vehicle for 24 h. Following treatment, whole cells were collected, and luciferase activity was determined using the Steady-Glo Luciferase Assay System (Promega; 72530). Similarly, cells were transfected with a CMV-promoter-GFP-PGC-1α-reporter plasmid using the same transfection procedure as described above. This is a constitutively active plasmid, expressing PGC-1α bound to GFP, permitting the observation of PGC-1α localization.

Statistical Analysis

All graphs were produced, and statistics were analyzed using the GraphPad Prism software (ver. 8) and represented as means ± SE. For comparisons between vehicle and SFN with respect to nuclear-cytosolic fractions, confocal imaging, and certain whole cell analyses as specified within figure captions, a two-tailed unpaired *t* test was performed, assuming normal parametric distribution. A two-way analysis of variance (ANOVA) was completed followed by a Tukey's post hoc test for the analysis of oxygen consumption, PGC-1α promoter activity, reactive oxygen species measurements, MG132 treatment, and protein analysis following chronic contractile activity, and rotenone treatment. Data were considered significant when $P < 0.05$.

RESULTS

Sulforaphane Increases Nrf-2 Accumulation and Nuclear Localization

SFN has been well documented as a potent inducer of the Nrf-2-ARE axis by directly modifying Keap1, the negative regulator of Nrf-2. To examine the upstream activation of this pathway, myotubes were treated with SFN for 24 h and collected. Whole cell lysates revealed a sixfold increase in Nrf-2 protein ($P < 0.0001$) relative to vehicle-treated cells, indicating Nrf-2 accumulation (Fig. 1, *A* and *C*). To determine

whether this transcription factor was translocating to the nucleus to enhance the upregulation of target genes, nuclear-cytosolic fractions were prepared, which demonstrated an 11-fold increase in nuclear Nrf-2 (Fig. 1, *B* and *C*; $P < 0.0001$). This was accompanied by a reduction in Keap1 ($P = 0.0129$) and a two-fold increase in p62 ($P = 0.0051$), an autophagy receptor that facilitates the removal of cellular cargo (Fig. 1, *A* and *C*).

Sulforaphane Enhances Mitochondrial Content and Respiration

Nrf-2 has been reported to increase mitochondrial biogenesis through its own action, as well as via its downstream effectors, including NQO1 and HO-1. To evaluate if SFN may be able to augment Nrf-2-mediated biogenesis within skeletal muscle cells, Western blotting and flow cytometry experiments were performed to detect changes in mitochondrial content following treatment. After 24 h, there was a sevenfold increase in TFAM ($P = 0.0099$), an important mediator of mtDNA replication. This was accompanied by a 1.5-fold increase in COX I ($P < 0.0095$), a subunit of Complex IV of the electron transport chain (ETC), and a 1.6-fold increase in MFN2 ($P < 0.0476$), a key protein involved in mitochondrial fusion, by 48 h (Fig. 2, *A* and *B*). At the same time point, flow cytometry revealed a 12-fold increase in mitochondrial mass and a 1.3-fold increase in membrane potential using MitoTracker Green ($P = 0.0013$) and MitoTracker Red ($P = 0.0041$), respectively (Fig. 2, *C* and *D*). Assessment of mitochondrial respiration parameters, including basal respiration (SFN $P < 0.0001$), ATP-linked respiration (SFN $P < 0.0001$), uncoupled respiration using FCCP (SFN $P = 0.0006$), and spare respiration (SFN $P = 0.0006$) demonstrated a main effect of treatment. No effect of time was observed, revealing the same enhancement in respiration at both 24 h and 48 h (Fig. 3*A*). Furthermore, confocal imaging corroborated the flow cytometry data, demonstrating a significant increase in mitochondria with their membrane potential intact, evident through enhanced colocalization of Mitotracker Green and MitoTracker Red (Fig. 3, *B* and *C*; $P < 0.0001$).

Sulforaphane Pretreatment Blunts Rotenone-Induced Oxidative Stress through the Activation of Antioxidant Enzymes Related to the Nrf-2-ARE Axis

After observing an 11-fold increase in nuclear Nrf-2, we sought to evaluate if SFN may be able to enhance the activation of downstream antioxidant proteins related to the Nrf-2-ARE axis and confer cellular and mitochondrial protection against oxidative stress. Cells were pretreated with SFN for 24 h, followed by a 24-h cotreatment with rotenone, an inhibitor of Complex I of the ETC (Fig. 4*A*). Previous reports have shown that rotenone is a powerful inducer of mitochondrial-mediated oxidative stress, leading to cellular dysfunction (51). Following SFN treatment, Western blotting revealed a significant increase in glutathione reductase (GR; SFN $P = 0.0008$), glucose-6-phosphate-dehydrogenase (G6PD; SFN $P = 0.0003$), NAD(P)H Quinone Oxidoreductase (NQO1; SFN $P < 0.0001$), catalase (CAT; SFN $P < 0.0001$) and glutathione peroxidase-1 (GPX-1; SFN $P = 0.0160$) protein (Fig. 4, *B* and *C*). CAT (ROT $P = 0.0015$) and GPX-1 (ROT $P = 0.0136$) were both upregulated following rotenone, while an interaction effect was observed when combining ROT and SFN for CAT (SFN × ROT $P = 0.0255$) and GPX-1 (SFN × ROT $P = 0.0228$; Fig. 4, *B* and *C*).

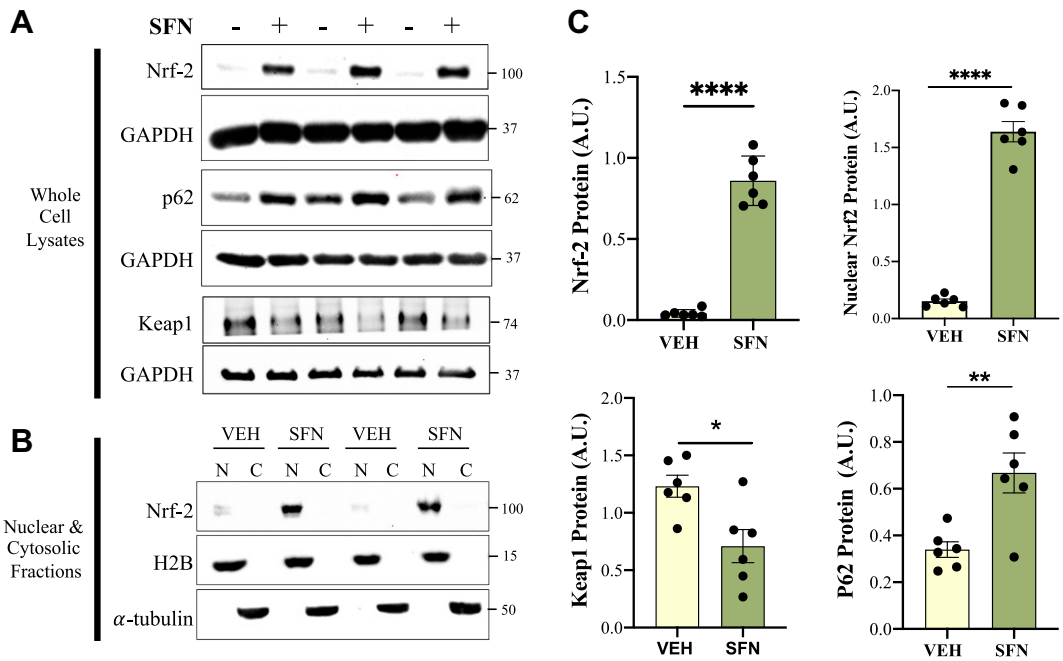

Figure 1. Expression of upstream proteins involved in the Nrf-2-ARE antioxidant axis following 24-h SFN treatment. *A* and *C*: representative Western blots and quantifications of Nrf-2 (****$P < 0.0001$), p62 (**$P < 0.01$), and Keap1 (*$P < 0.05$), normalized to the corresponding GAPDH in whole cell lysates ($n = 6$). Negative (−) indicates cells were treated with vehicle. *B* and *C*: representative nuclear (N)-cytosolic (C) Western blot of Nrf-2 (****$P < 0.0001$) and corresponding quantification. Nrf-2 was normalized to H2B for the nuclear fraction, and purity was evaluated with α-tubulin. An unpaired two-tailed *t* test was performed for each graph ($n = 6$), and all values are represented as ±SE. ARE, antioxidant response element; H2B, Histone 2B; Nrf-2, nuclear factor erythroid 2-related factor 2; SFN, Sulforaphane; VEH, vehicle.

AJP-Cell Physiol • doi:10.1152/ajpcell.00669.2024 • www.ajpcell.org

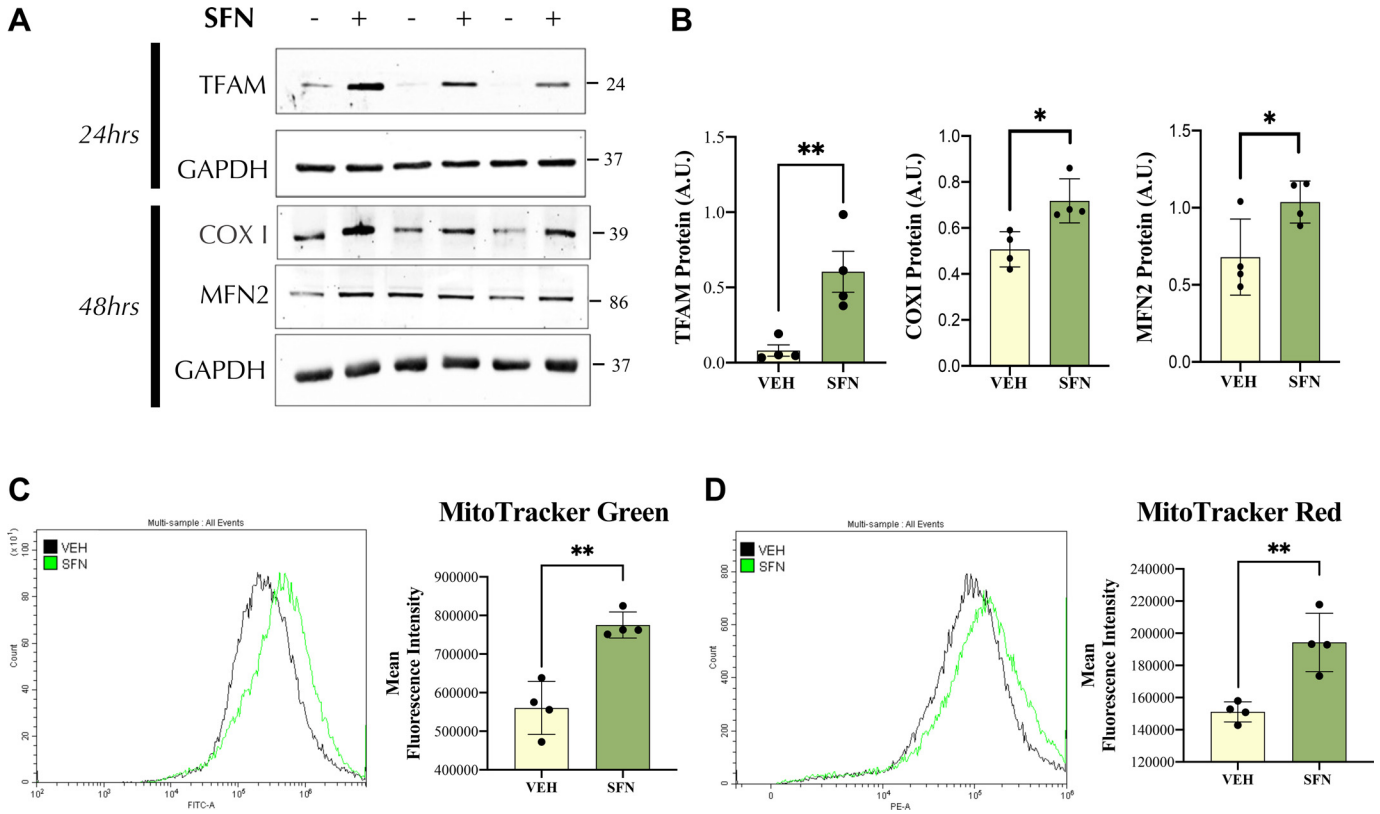

Figure 2. Mitochondrial content following SFN. *A*: representative Western blots of TFAM following 24-h SFN, as well as mitochondrially encoded COX I, and the fusion-related protein MFN2 following 48-h SFN, resupplemented at 24 h. *B*: Western blot quantifications of TFAM ($n = 4$, $^{**}P < 0.01$), COX I ($n = 4$, $^{*}P < 0.05$), and MFN2 ($n = 4$, $^{*}P < 0.05$). All targets were normalized to GAPDH. *C* and *D*: representative histogram and corresponding quantification of MitoTracker Green, for a measure of total mitochondrial content ($n = 4$, $^{**}P < 0.01$) and MitoTracker Red, as a functional measurement. Three technical replicates were completed for each *n*. An unpaired two-tailed *t* test was performed for each graph. All values are represented as ± SE. SFN, Sulforaphane; VEH, vehicle; TFAM, mitochondrial transcription factor A.

To determine if alterations in antioxidant proteins may be able to provide a rescue effect in terms of ROS, cellular and mitochondrial ROS were detected with CellROX Green and MitoSOX Red, respectively, along with MitoTracker Red (MTR) to evaluate membrane potential. Although SFN treatment did not significantly alter cellular ROS basally ($P = 0.051$; Fig. 4*D*), there was a 27% reduction in mitochondrial ROS (SFN $P = 0.0008$; Fig. 4*E*) and 24% increase in mitochondrial with their membrane potential intact (SFN $P = 0.0112$; Fig. 4*F*). Rotenone induced a 1.3-fold increase in cellular (ROT $P = 0.0037$; Fig. 4*D*) and 1.8-fold increase in mitochondrial (ROT $P < 0.0001$; Fig. 4*E*) ROS emission, along with a 23% reduction in membrane potential (ROT $P = 0.0474$; Fig. 4*E*). However, this oxidative stress was blunted with SFN pretreatment, evident through a 27% reduction in cellular ROS (SFN × ROT $P = 0.0257$; Fig. 4*D*) and 43% reduction in mitochondrial ROS (SFN × ROT $P < 0.0001$; Fig. 4*E*), as indicated through an interaction effect.

Sulforaphane Enhances PGC-1α Promoter Activity, Protein Accumulation, and Nuclear Localization

To evaluate the molecular mechanisms underpinning Nrf-2-mediated mitochondrial biogenesis, PGC-1α promoter activity was assessed to determine if there was an enhanced transcriptional drive for this regulator of mitochondrial biogenesis (Fig. 5*A*). Following transfection of a PGC-1α-promoter-luciferase-reporter plasmid, there was approximately a 15-fold increase in luciferase activity (PROM $P < 0.0001$) compared with the empty vector. After transfection of this plasmid and 24 h of SFN treatment, there was a 1.5-fold increase in promoter activity, evident through an interaction effect when combining the PGC-1α promoter plasmid with SFN (PROM + SFN $P = 0.0006$; Fig. 5*B*). To determine what may be causing an increase in promoter activity, transcription factors previously reported to enhance PGC-1α transcription were measured in nuclear and cytosolic fractions at the same timepoint promoter activity was observed (Fig. 5, *C* and *D*). SFN treatment enhanced the nuclear accumulation of SP1 ($P = 0.0012$) and CREB1 ($P = 0.0070$) by 1.8-fold and 1.7-fold, respectively, relative to vehicle-treated cells; however, no change was detected in USF-1 ($P = 0.117$) or ATF-2 ($P = 0.103$) protein.

To determine the subcellular localization and accumulation of PGC-1α, a CMV-promoter-GFP-PGC-1α-reporter construct was used. Following transfection, cells were cotreated with MG132, a proteasome inhibitor, to assess how treatment may augment PGC-1α accumulation (Fig. 6*A*). PGC-1α protein is very low basally; therefore, MG132 was required to begin with a larger pool of PGC-1α protein to assess any effect of SFN. We observed a main effect of SFN on PGC-1α accumulation (SFN $P = 0.0002$; Fig. 6*B*) and nuclear localization (SFN $P = 0.0059$; Fig. 6*C*) basally. However, this was not significant following the post hoc test, despite a 1.9-fold increase in PGC-1α. Upon

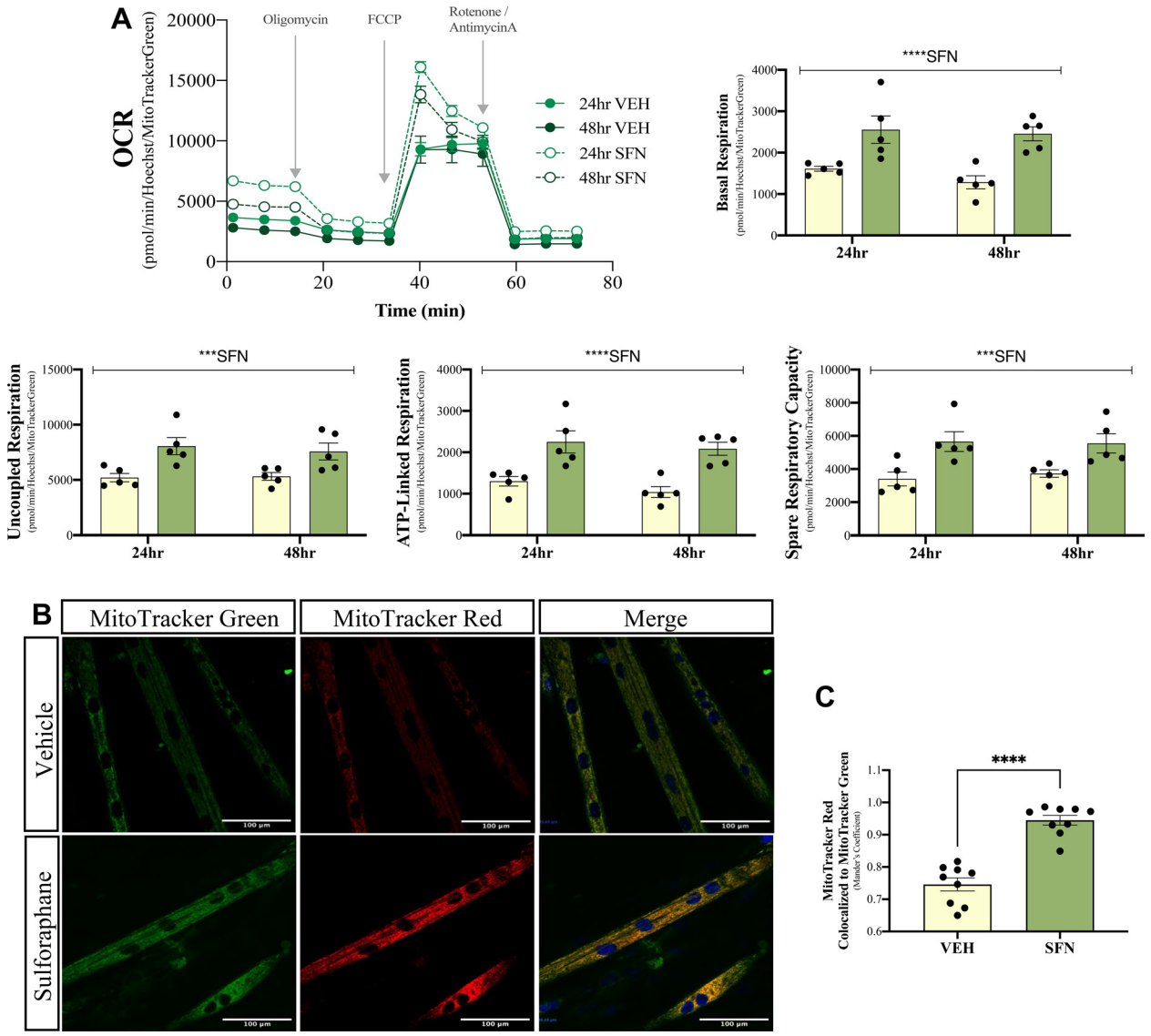

Figure 3. Mitochondrial respiration and functional parameters following SFN treatment. *A*: representative Seahorse oxygen consumption rate (OCR) tracing following the addition of substrates as shown, and the corresponding graphical quantifications following 24-h and 48-h SFN treatment. Cells were resupplemented with treatment at 24 h. Basal respiration, uncoupled respiration, ATP-linked respiration, and spare respiratory capacity were normalized to mitochondrial content and nuclei to obtain respiration per cell. A two-way ANOVA was performed for each graph to determine the effect of SFN and time ($n = 5$; ***$P < 0.001$, and ****$P < 0.0001$). "SFN" indicates a main effect of SFN; *P value of SFN; 23 technical replicates were completed for each n and performed across five independent experiments. *B* and *C*: representative confocal microscopy images of MitoTracker Green and Red following 48-h SFN or vehicle treatment (×60 magnification). Colocalization was determined using Mander's overlap coefficient (****$P < 0.0001$), evaluating the fraction of MitoTracker red localized to MitoTracker Green ($n = 9$; 2 to 3 myotubes per image). A two-tailed unpaired t test was performed. All values are represented as ± SE. SFN, Sulforaphane.

cotreatment with MG132, SFN elicited a 1.9-fold increase in PGC-1α accumulation (SFN + MG132 $P = 0.0041$; Fig. 6*B*) and a twofold increase in PGC-1α translocation to the nucleus (SFN + MG132 $P = 0.0021$; Fig. 6*C*). Although MG132 treatment elicited a sixfold increase in PGC-1αaccumulation (MG132 $P < 0.0001$; Fig. 6*B*), this did not result in its nuclear localization ($P = 0.9858$; Fig. 6*C*).

Next, to evaluate if there was any synergistic or additive effect of SFN treatment when combined with "exercise," an in vitro model of CCA was used (Fig. 7*A*), as previously outlined (10, 49, 50). Mitochondrial and lysosomal adaptations have been well documented both in vivo and in vitro, demonstrating that chronic muscle use enhances the synthesis of new mitochondria and lysosomes (24). Consistent with previous reports, our CCA model elicited a marked increase in TFAM (CCA $P = 0.0075$; Fig. 7, *B* and *C*) and TFE3 (CCA $P = 0.0002$; Fig. 7, *B* and *C*). There was a main effect of SFN (SFN $P < 0.0001$; Fig. 7, *B* and *C*) treatment alone, as well as an interaction effect (SFN + CCA $P = 0.0066$; Fig. 7, *B* and *C*) on TFAM protein expression. There was a significant increase in TFE3 protein relative to untreated cells ($P = 0.0033$; Fig. 7, *B* and *C*), which was accompanied by an increase in mitochondrial and lysosomal-related proteins. There was a main effect of CCA and SFN on mitochondrial markers including COX I (CCA $P = 0.0037$, SFN $P < 0.0001$), UQCRC2 (CCA $P = 0.0246$, SFN $P = 0.0026$), and VDAC (CCA $P = 0.0305$, SFN $P < 0.0007$), as well as Mature Cathepsin B, a lysosomal protease that cleaves cellular cargo (CCA $P = 0.0345$, SFN $P = 0.0035$). To evaluate lysosomal

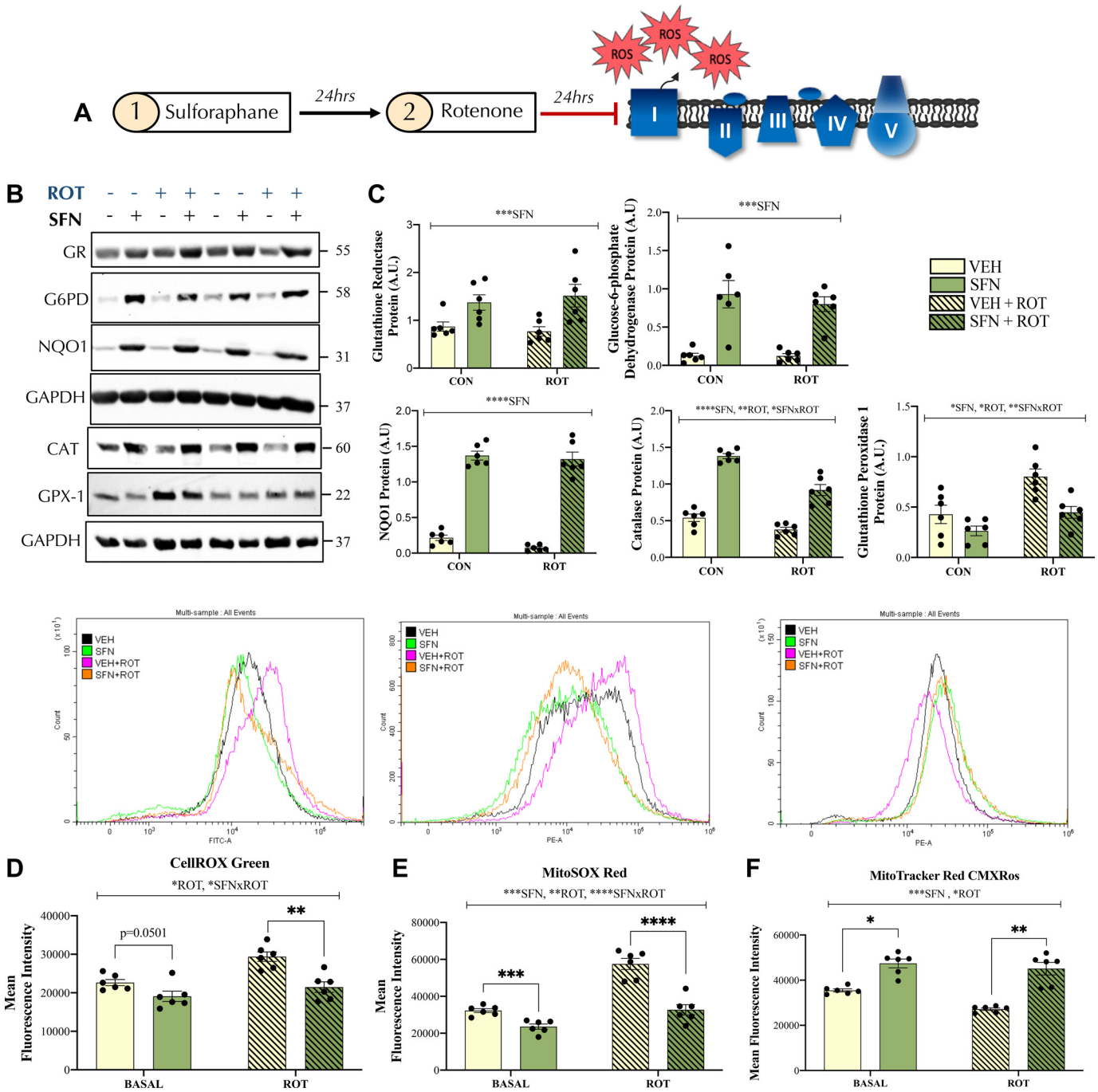

Figure 4. Antioxidant proteins and ROS with SFN pretreatment followed by rotenone. *A*: schematic depicting treatment. Myotubes were pretreated with SFN or vehicle for 24 h before coincubation with 150 nM rotenone (ROT), a complex 1 inhibitor, for 24 h to induce oxidative stress. *B* and *C*: representative Western blots and corresponding quantifications of Glutathione Reductase (GR), Glucose-6-Phosphate Dehydrogenase (G6PD), NAD(P)H Quinone Oxidoreductase (NQO1), Catalase (CAT), and Glutathione Peroxidase-1 in whole cell lysates. All targets were normalized to GAPDH ($n = 6$). *D–F*: representative histograms and mean fluorescence intensity quantifications of CellROX Green, MitoSOX Red, and Mitotracker Red detected via flow cytometry ($n = 6$). Three technical replicates were completed for each *n*. A two-way ANOVA was performed for all graphs to determine the effect of SFN and ROT. Statistics are shown as follows: "SFN" is the main effect of SFN, "ROT" is the main effect of rotenone "SFN × ROT" reflects an interaction effect between SFN and ROT; *P value for each effect. *$P < 0.05$, **$P < 0.01$, ***$P < 0.001$, and ****$P < 0.0001$. All values are represented as ± SE. ROT, rotenone; SFN, Sulforaphane; VEH, vehicle.

degradation capacity, and therefore assess lysosomal function, a ratio of mature:premature Cathepsin B was determined following interventions. This functional metric revealed that CCA promoted lysosomal function by 22% relative to unstimulated cells (CCA $P = 0.052$), consistent with previous reports (26, 49). Furthermore, the lysosomal membrane protein vATPase, used as a measure of lysosomal mass, was also enhanced following SFN treatment (SFN $P = 0.0001$; Fig. 7, *B* and *C*).

Chronic exercise has been shown to enhance the levels of antioxidant proteins, which are essential for the reduction in

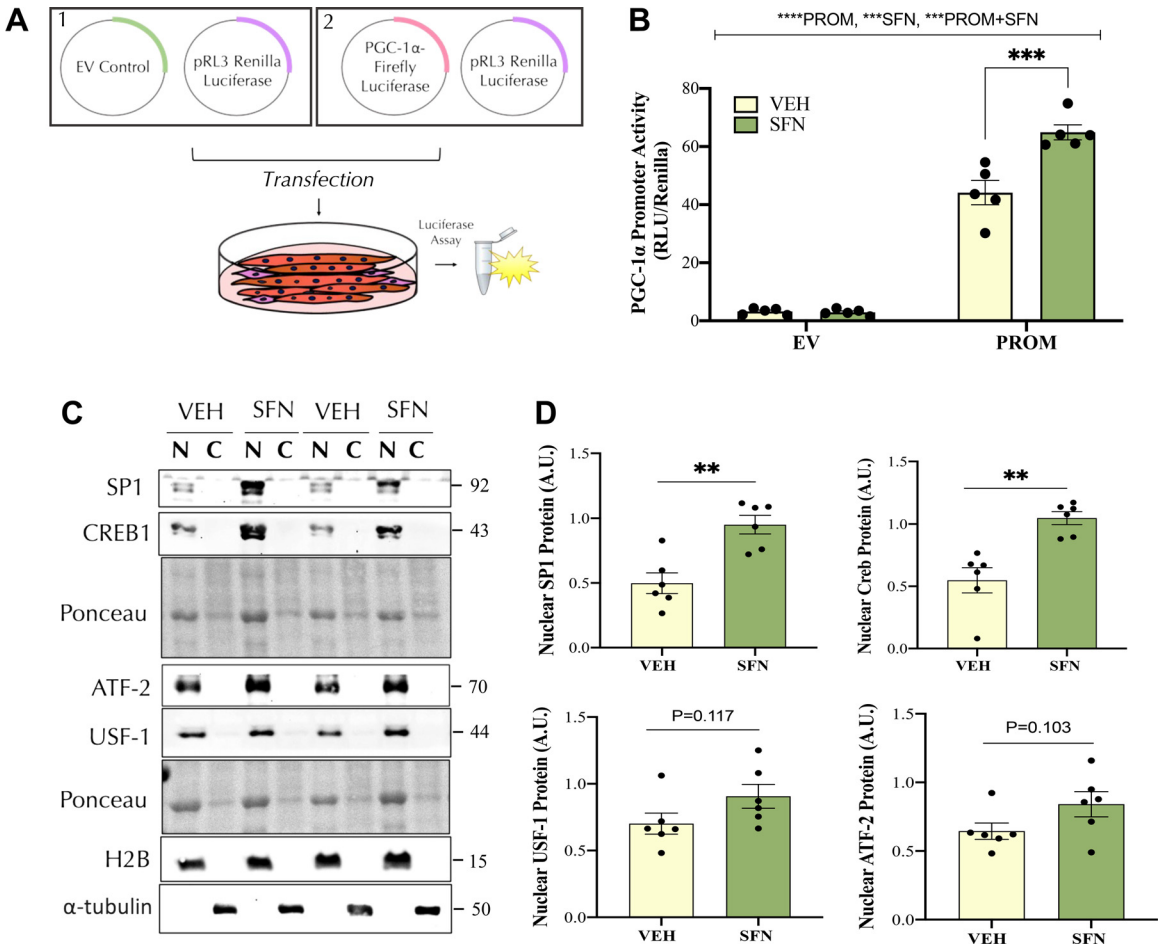

Figure 5. Transcriptional drive toward PGC-1α following SFN treatment. *A*: graphical representation of plasmids used for transfection and subsequent luciferase assay. Myotubes were transfected with either an empty vector (EV) or a PGC-1α-promoter-firefly-luciferase-reporter plasmid. In both instances, cells were cotransfected with a CMV-promoter-renilla-luciferase-reporter plasmid (pRL3) to control for transfection efficiency. *B*: PGC-1α promoter activity was measured as relative light units (RLU), normalized to Renilla Luciferase ($n = 5$). Two technical replicates were completed for each *n*. A two-way ANOVA was performed to determine the effect of the PGC-1α promoter and SFN. Statistics are shown as follows: "PROM" is the main effect of PGC-1α promoter, "SFN" is the main effect of SFN, "PROM + SFN" is the interaction effect between PGC-1α promoter and SFN treatment. *P value for each effect. **$P < 0.01$, ***$P < 0.001$, and ****$P < 0.0001$. *C* and *D*: representative nuclear (N)-cytosolic (C) Western blots and corresponding quantification of SP1 (**$P < 0.01$), CREB1 (**$P < 0.01$), USF-1 ($P = 0.117$), and ATF-2 ($P = 0.103$). All targets were normalized to ponceau, and purity was evaluated with H2B and α-tubulin ($n = 6$). Significance was determined with a two-tailed unpaired *t* test for each graph. All values are represented as ± SE. H2B, Histone 2B; SFN, Sulforaphane.

ROS observed with training (52). We were able to confirm that our model of CCA, and SFN, elicited an accumulation of antioxidant proteins, including NQO1 (CCA $P < 0.0001$, SFN $P < 0.0001$; Fig. 8, *A* and *B*), GR (CCA $P = 0.0289$, SFN $P = 0.0003$; Fig. 8, *A* and *B*), and GPX-1 (CCA $P = 0.0063$, SFN $P < 0.0001$; Fig. 8, *A* and *B*). SFN also elicited a robust enhancement in CAT (SFN $P < 0.0001$; Fig. 8, *A* and *B*) and G6PD (SFN $P < 0.0001$; Fig. 8, *A* and *B*) protein, whereas an interaction effect was observed for NQO1 (SFN + CCA $P < 0.0001$; Fig. 8, *A* and *B*), HO-1 (SFN + CCA $P = 0.0067$; Fig. 8, *A* and *B*), and GPX-1 protein (SFN + CCA $P = 0.0024$; Fig. 8, *A* and *B*) when combining the two interventions. These protein changes had direct functional consequences on cellular and mitochondrial ROS, evident through 38 and 36% reductions in cellular ROS following CCA and SFN, respectively (CCA $P = 0.0017$, SFN $P = 0.0035$; Fig. 10*C*). Similarly, mitochondrial ROS was reduced by 23 and 22% with CCA and SFN, respectively (CCA $P = 0.0028$, SFN $P = 0.0040$; Fig. 8*D*). Furthermore, upon combining CCA and SFN, there was an 11% greater reduction in mitochondrial ROS relative to vehicle-treated stimulated cells (Fig. 8*D*).

Effects of Sulforaphane on Mitochondrial Morphology When Combined with CCA

Since our data revealed an effect of SFN on mitochondrial content (Figs. 2 and 7), we sought to investigate if mitochondrial dynamics may be altered as well. To examine this, mitochondrial morphology was observed via confocal microscopy, and images were skeletonized to visualize mitochondrial length, branching, and interconnectedness, as well as Western blotting to examine fusion and fission-related proteins. Although Western blotting did not reveal any difference in MFN2 (SFN $P = 0.2368$; Fig. 9, *A* and *B*), a fusion-related protein, there were significant alterations to DRP1, a protein recruited to the mitochondria for fission-related processes (SFN $P < 0.0001$; Fig. 9, *A* and *B*). Indeed, a two-way ANOVA revealed a main effect of

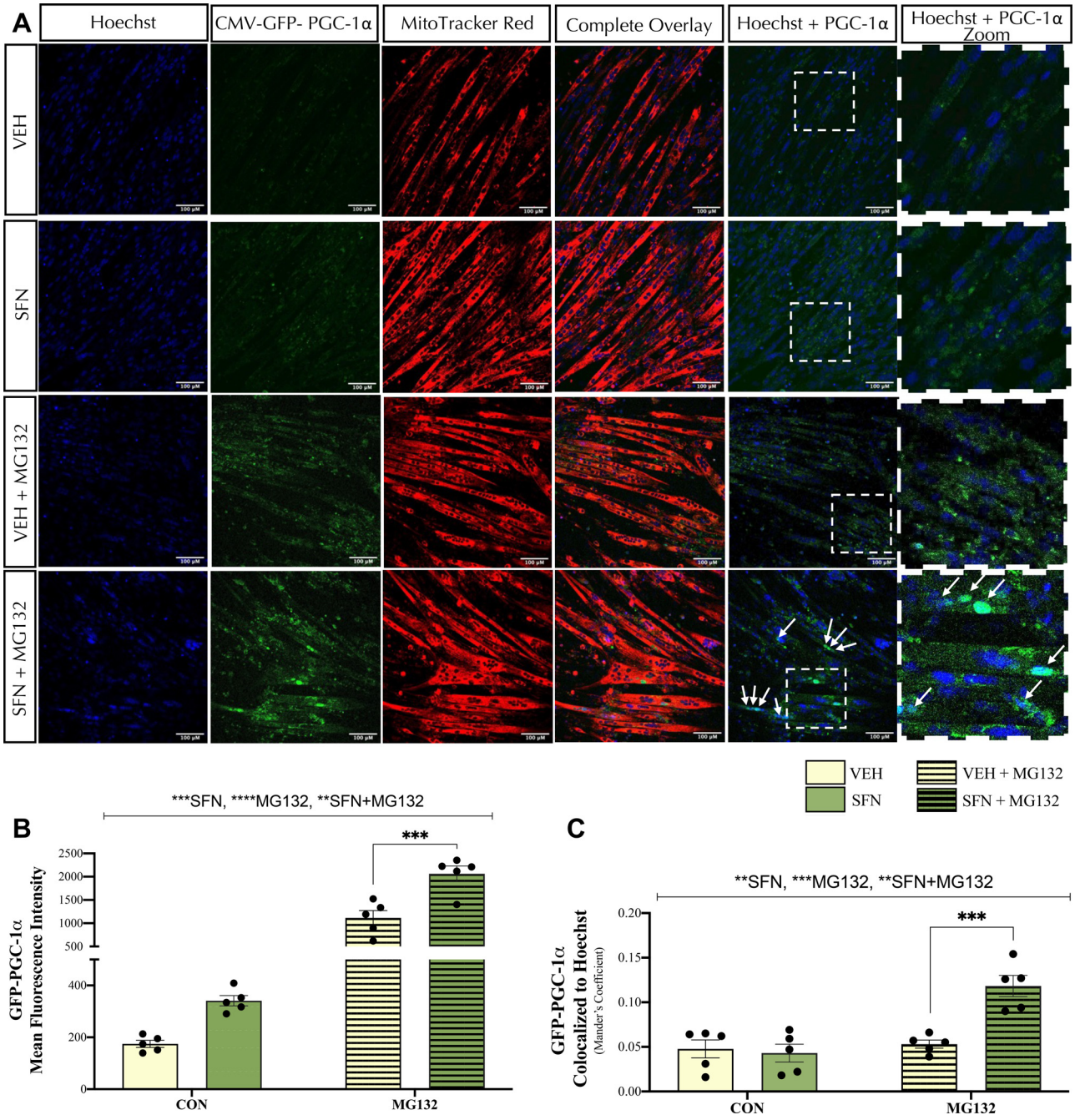

Figure 6. PGC-1α accumulation and nuclear localization following SFN. *A*: representative confocal images (×20 magnification) of vehicle (VEH), sulforaphane (SFN), VEH + MG132, and SFN + MG132 treated myotubes following 6 h of treatment. Cells were immediately stained with Hoechst and MitoTracker Red ($n = 5$; roughly 15–20 myotubes per image). Hoechst and PGC-1α overlay along with an *inset* enlarged by ×2.8 are provided to offer better visualization of nuclear PGC-1α indicated by white arrows. *B*: mean fluorescence intensity of GFP was detected to measure PGC-1α accumulation. *C*: colocalization of GFP to Hoechst was determined using Mander's overlap coefficient. A two-way ANOVA was performed to evaluate the effect of SFN and MG132. Statistics are as follows: "SFN" is the main effect of SFN, "MG132" is the main effect of MG132, and "SFN + MG132" is the interaction effect between SFN and MG132. *P value for each effect. **$P < 0.01$, ***$P < 0.001$, and ****$P < 0.0001$. All values are represented as ± SE.

SFN (SFN $P < 0.0001$; Fig. 9, *A* and *B*) and CCA (CCA $P < 0.0001$; Fig. 9, *A* and *B*), along with an interaction effect between the two variables (SFN + CCA $P < 0.0001$; Fig. 9, *A* and *B*). Mitochondrial length (SFN $P < 0.0001$; Fig. 9, *C* and *D*) and the number of branch junctions (SFN $P < 0.0001$; Fig. 9, *C* and *E*) were also enhanced by 3- and 2.2-fold, respectively, following SFN treatment.

Sulforaphane Transiently Increases Cellular ROS and Activates Upstream Kinases Consistent with Acute Contractile Activity

To elucidate the precise mechanisms underlying Nrf-2 activation and alterations in mitochondrial content, ROS were evaluated following 3 h of SFN treatment. We were able to

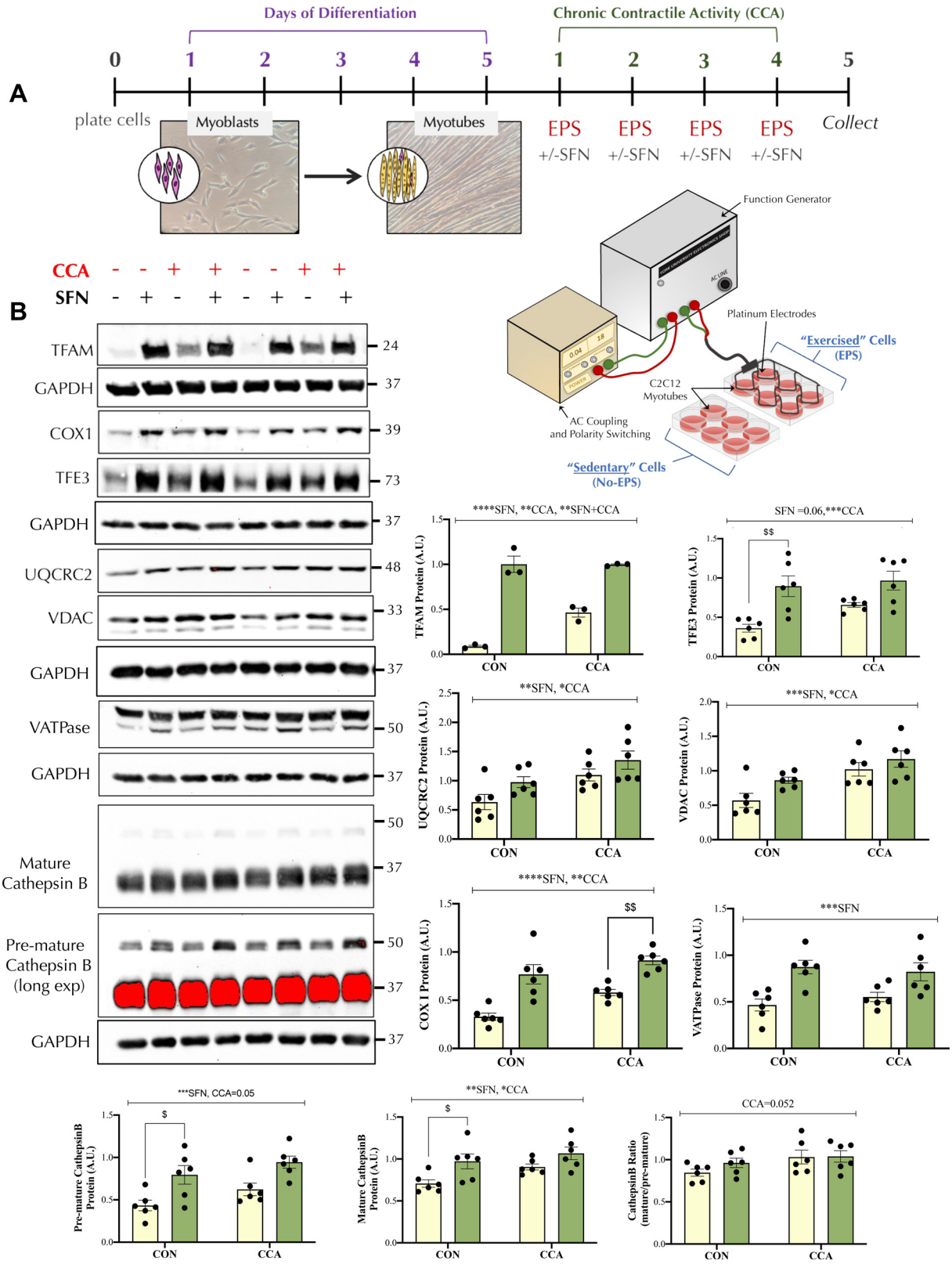

AJP-Cell Physiol • doi:10.1152/ajpcell.00669.2024 • www.ajpcell.org

detect a significant increase in cellular ROS ($P = 0.0018$; Fig. 10*A*) with no change in mitochondrial ROS ($P = 0.3130$; Fig. 10*B*). Interestingly, this alteration appeared to be transient, as cellular ROS was no longer elevated by 24 h (Fig. 8*C*). To determine what kinases may be responsive to this transient increase in ROS, an acute bout of contractile activity was performed to evaluate the expression of ROS-sensitive kinases involved in mitochondrial biogenesis and Nrf-2 activation. AMPK (ACA $P < 0.0001$; Fig. 10, *C* and *D*) and JNK (ACA $P < 0.0001$; Fig. 10, *C* and *D*), two kinases that have been well documented to be upregulated with acute exercise, were significantly activated with our model of acute contractile activity. Other upstream kinases, including CAMK (ACA $P < 0.0001$; Supplemental Fig. S2) and P38 MAPK (ACA $P < 0.0001$; Supplemental Fig. S2) were also upregulated, demonstrating the sensitivity of these kinases to exercise-induced secondary messengers. Interestingly, we observed a fivefold increase in AMPK activation (SFN $P = 0.0312$; Fig. 10, *C* and *D*) and a fourfold increase in JNK1 activation (SFN $P = 0.0115$; Fig. 10, *C* and *D*), activation following 3 h of SFN treatment alone (Fig. 10).

DISCUSSION

Mitochondria are critical organelles that play a pivotal role in the maintenance of skeletal muscle cellular homeostasis (5, 23, 52). However, mitochondrial profiles in muscle can be altered under a variety of disease conditions as well as with age (5, 52), thereby highlighting the importance of investigating novel approaches to refresh and enhance the mitochondrial pool. The purpose of this study was to investigate the potential role of the natural plant compound SFN in improving the mitochondrial phenotype through the activation of mitochondrial biogenesis and by increasing organelle antioxidant capacity. To further examine if the signaling cascades activated in response to SFN were common to those typically activated by exercise, we combined SFN treatment with a model of CCA of myotubes, which typically results in beneficial mitochondrial adaptions (25, 49).

Previous work has shown that SFN increases the expression of antioxidant enzymes by activating the Nrf-2-Keap1 axis (31, 38). Upon SFN-mediated modifications to Keap1, Nrf-2 accumulates and translocates to the nucleus to bind to ARE regions upstream of target genes (36, 38, 39). We found that SFN induced a robust accumulation of whole cell as well as nuclear-localized Nrf-2 protein, likely mediating the upregulation of antioxidant proteins observed. Cytosolic kinases AMPK (53) and JNK (54) have been reported to phosphorylate Nrf-2 and permit its release from Keap1. In both instances, these phosphorylation events enhance the translocation and nuclear retention of Nrf-2. To evaluate the activation of these kinases and determine if they may be implicated in Nrf-2's mechanism of action, we evaluated ROS content and kinase phosphorylation after 3 h of treatment. Interestingly, we observed an elevation in cellular ROS and activation of AMPK and JNK1, similar to others (55, 56). Given that ROS have been reported to activate both AMPK and JNK, this suggests the possibility that SFN transiently increases ROS, driving kinase activation, which may subsequently phosphorylate Nrf-2 and permit its release from Keap-1 for nuclear translocation. In addition, Nrf-2 nuclear translocation coincided with a marked reduction in Keap1 and an increase in p62 protein. Other groups have shown that Keap1 is removed through autophagy-mediated mechanisms (57, 58) and that Nrf-2 signaling enhances autophagy initiation (59, 60). These changes in protein levels suggest that Nrf-2 may elicit a p62-dependent positive feedback loop, to further confer Nrf-2 accumulation and signaling through the removal of Keap1 via autophagy (61, 62).

Nrf-2 regulates antioxidant enzyme expression by directly increasing target gene transcription. To investigate if this may have functional consequences on mitochondrial preservation, cells were pretreated with SFN, followed by a cotreatment with rotenone to induce mitochondrial dysfunction and oxidative stress. Consistent with this signaling axis, Nrf-2 enhanced the expression of several antioxidant enzymes such as catalase and glutathione reductase. Interestingly, these protein changes were sustained under rotenone-induced oxidative stress and served to blunt excessive cellular ROS. Importantly, this was accompanied by a reduction in mitochondrial ROS and an increase in membrane potential, together suggesting that SFN can protect mitochondrial function under oxidative stress, highlighting the therapeutic potential of this agent. These functional enhancements were further exemplified when examining respiration, which demonstrated an increase in basal oxygen consumption occurring after only 24 h, which persisted by 48 h. Confocal microscopy corroborated these functional enhancements, demonstrating an increase in the colocalization of MitoTracker Green and MitoTracker Red, suggesting that there was a greater amount of mitochondria present that also had an intact membrane potential following SFN. As mitochondrial fusion can lead to functional improvements, we sought to evaluate whether mitochondrial morphology may be driving the changes observed. Although we were unable to detect any difference in MFN2, a pro-fusion protein, we observed a significant reduction in the pro-fission protein Drp-1. Furthermore, confocal microscopy revealed greater mitochondrial length and number of junctions per mitochondria with treatment, together suggesting that SFN enhances the interconnectedness of the mitochondrial reticulum by reducing fission processes. Indeed, previous studies have shown that SFN reduces Drp-1 protein (63) and recruitment to the mitochondria (64), further suggesting that this axis exists.

Figure 7. Mitochondrial and lysosomal-related proteins following CCA. *A*: schematic demonstrating the "exercise-in-a-dish" experimental model. Myoblasts were plated and differentiated into myotubes. Following differentiation, myotubes were subjected to 3 h of electrical pulse stimulation (EPS) followed by a 21-h recovery, where they were supplemented with either vehicle or SFN. *B*: representative Western blots and corresponding quantifications of TFAM, COX I, TFE3, UQCRC2, VDAC, vATPase, and Cathepsin B. All targets were normalized to GAPDH. The ratio of mature Cathepsin B to premature was assessed as an indication of lysosomal function. A two-way ANOVA was performed for all graphs to determine the effect of SFN and CCA. Statistics are shown as follows: "SFN" is the main effect of SFN, "CCA" is the main effect of CCA, and "SFN + CCA" is the interaction effect between SFN and CCA. *P value for each effect. *$P < 0.05$, **$P < 0.01$, ***$P < 0.001$, and ****$P < 0.0001$; $Post hoc analyses indicating significance to the corresponding group; $$$P < 0.01$. All values are represented as ± SE ($n = 6$). CCA, chronic contractile activity; SFN, Sulforaphane; TFAM, mitochondrial transcription factor A.

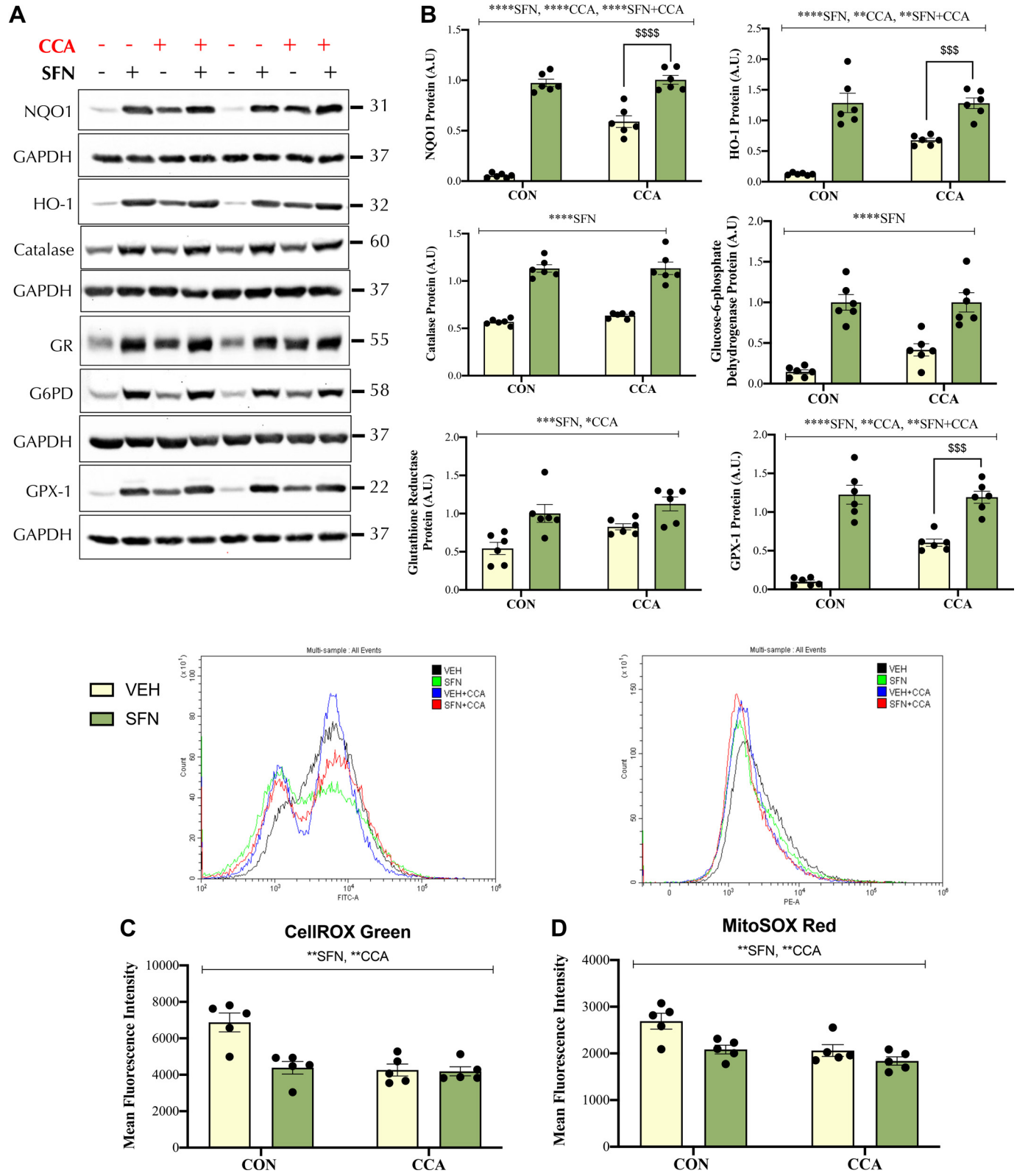

Figure 8. Antioxidant proteins and ROS following CCA. *A* and *B*: representative Western blots and the corresponding quantification for NQO1, heme oxygenase-1 (HO-1), catalase (CAT), glutathione reductase (GR), glucose-6-phosphate-dehydrogenase (G6PD), and glutathione peroxidase-1 (GPX-1) following CCA. All targets were normalized to GAPDH ($n = 6$). *C* and *D*: CellROX Green and MitoSOX Red mean fluorescence intensity was detected via flow cytometry, as shown with representative histograms and graphical quantifications ($n = 5$). Three technical replicates were completed for each *n*. A two-way ANOVA was performed for all graphs to determine the effect of SFN and CCA. Statistics are shown as follows: "SFN" is the main effect of SFN, "CCA" is the main effect of CCA, and "SFN + CCA" is the interaction effect between SFN and CCA. *P value for each effect. *$P < 0.05$, **$P < 0.01$, ***$P < 0.001$, and ****$P < 0.0001$. \$\$\$ < 0.001, \$\$\$\$ <0.0001. All values are represented as ± SE. CCA, chronic contractile activity; ROS, reactive oxygen species; SFN, Sulforaphane.

AJP-Cell Physiol • doi:10.1152/ajpcell.00669.2024 • www.ajpcell.org

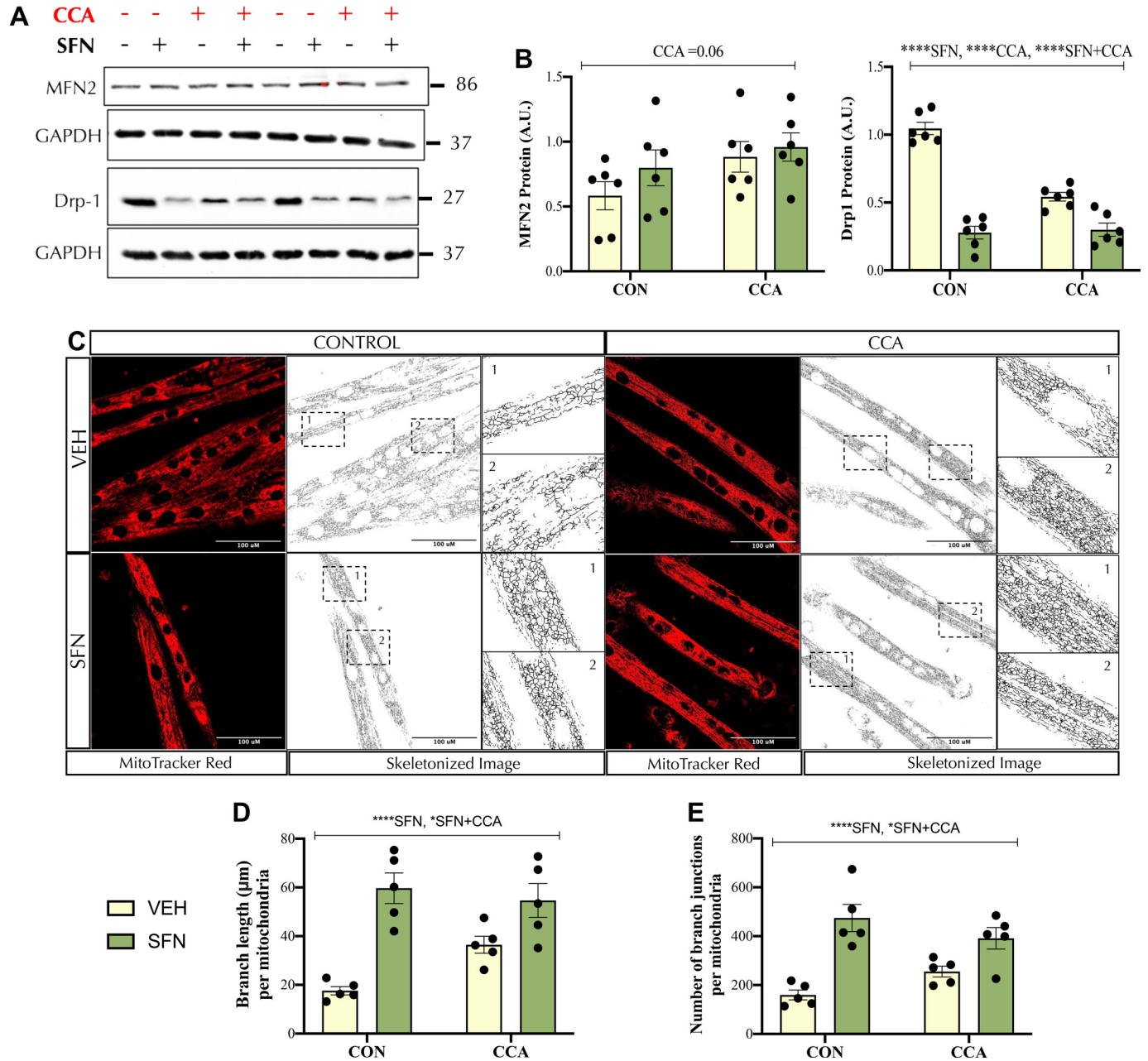

Figure 9. Mitochondrial dynamics following CCA. *A* and *B*: representative Western blots and corresponding quantifications of Mitofusin 2 (MFN2) and Dynamin-related protein-1 (Drp-1), both normalized to GAPDH ($n = 6$). *C*: representative confocal images (×60 magnification) of myotubes stained with MitoTracker Red, subsequently skeletonized using ImageJ to illustrate mitochondrial morphology. Two insets numbered 1 and 2 are enlarged by ×2.6 for each image to better visualize branching. *D* and *E*: quantifications of mitochondrial branch length and the number of branch junctions per mitochondrion. One branch junction is defined as a point in the reticulum where three or more branches meet ($n = 5$). Three images were analyzed for each *n*. A two-way ANOVA was performed for all graphs to determine the effect of SFN and CCA. Statistics are shown as follows: "SFN" is the main effect of SFN, "CCA" is the main effect of CCA, and "SFN + CCA" is the interaction effect between SFN and CCA. *P value for each effect. *$P < 0.05$ and ****$P <$ 0.0001. All values are represented as ± SE. CCA, chronic contractile activity; SFN, Sulforaphane.

Alongside functional and morphological improvements, we observed an increase in mitochondrial content and the signaling toward biogenesis, evident from an increase in TFAM and several mitochondrial-related proteins such as UQCRC2 and VDAC. This elevation in content is likely mediated in part by direct binding of Nrf-2 to ARE elements found upstream of NRF-1, a transcription factor well known for its role in TFAM expression (42), as well as other nuclear genes encoding mitochondrial proteins (65). Furthermore, overexpression of the downstream Nrf-2 target HO-1 has also been shown to increase PGC-1α and TFAM protein (66), whereas knockout significantly reduced total mitochondrial content and respiration (67), together suggesting that Nrf-2 signaling may play a role in mitochondrial biogenesis. To determine if Nrf-2-directed mitochondrial biogenesis was mediated by PGC-1α, a PGC-1α-promoter-luciferase-reporter construct was used. Our results demonstrated an increase in promoter activity following SFN treatment, indicating a strong drive toward

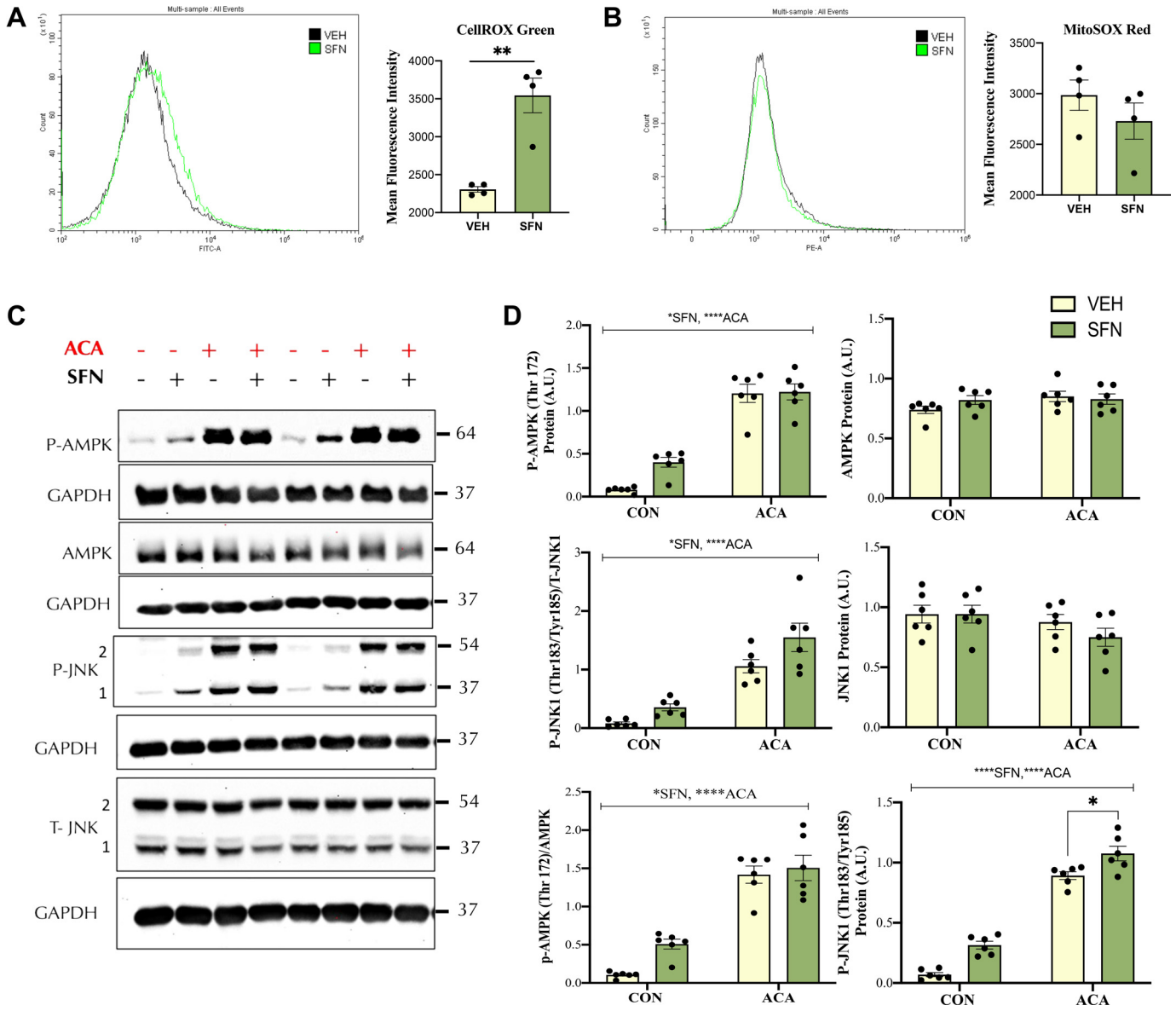

Figure 10. ROS and upstream kinase activation in response to acute contractile activity (ACA). *A* and *B*: representative histogram and quantification of CellROX green and MitoSOX Red following 3 h of treatment ($n = 4$). Three technical replicates were completed for each *n*. Significance was determined using a two-tailed unpaired *t* test. *C* and *D*: representative Western blots and corresponding quantifications of phospho-AMPK, total-AMPK, phospho-JNK, and total-JNK. All targets were normalized to GAPDH ($n = 6$). To obtain a measure of kinase activation, phosphorylated targets were normalized to the total kinase protein present. A two-way ANOVA was performed for all graphs to determine the effect of SFN and ACA. Statistics are shown as follows: "SFN" is the main effect of SFN and "ACA" is the main effect of ACA. *P value for each effect. $*P < 0.05$, $**P < 0.01$, and $****P < 0.0001$. All values are represented as ± SE. ACA, acute contractile activity; SFN, Sulforaphane.

biogenesis. Isolation of nuclear fractions revealed a marked increase in Nrf-2 as noted above, which likely binds to putative ARE sites within the PGC-1α promoter. Furthermore, SFN elicited an increase in the nuclear retention of transcription factors that have both been previously reported to bind and enhance PGC-1α promoter activity including Sp1 (50, 68) and CREB (15, 69), suggesting that SFN mediates biogenesis through multiple mechanisms.

To assess if PGC-1α was entering the nucleus to coactivate transcription factors involved in the expression of mitochondrial-related genes, a CMV-promoter-GFP-PGC-1α reporter plasmid was used. As PGC-1α has been classified as an intrinsically disordered protein (70), it is routinely targeted toward the proteasome for destruction, maintaining extremely low levels basally. To evaluate PGC-1α accumulation and to ensure the reliability of our PGC-1α measurements, the proteasome inhibitor MG132 was used. MG132 treatment resulted in an increase in whole cell PGC-1α levels as expected, whereas nuclear translocation remained unchanged, suggesting that PGC-1α levels are tightly regulated by proteasome activity. Interestingly, SFN enhanced PGC-1α nuclear translocation in the presence of MG132. This suggests that SFN may help attenuate PGC-1α decay possibly through the induction of NQO1 (see Fig. 4), a well-documented downstream target of Nrf-2 (58), which has been shown to bind to PGC-1α and protect it from the 20S proteasome, thereby increasing its half-life (70). NQO1 also

physically associates with the 20S proteasome, where it blunts proteolytic activity, therefore further reducing PGC-1α degradation (70, 71). These modifications could permit a high concentration gradient and sufficient time for SFN-induced AMPK phosphorylation of PGC-1α, permitting its nuclear localization; however, the precise mechanisms underlying this finding must be further evaluated.

Exercise training in vivo and CCA in animal and cellular models have been reported to enhance the expression of antioxidant proteins, increase mitochondrial content, and reduce mitochondrial ROS emission (24, 28). To determine the potential additive effects of SFN when combined with exercise, C2C12 myotubes were chronically stimulated and supplemented with SFN during their recovery period between bouts of contractile activity. As expected, and as shown previously, we established that our CCA model was effective in enhancing exercise-induced adaptations, including an increase in mitochondrial, lysosomal, and antioxidant-related proteins (24–26, 49). However, CCA did not further enhance SFN-mediated adaptations. There was no statistical difference between nonstimulated and stimulated cells treated with SFN for most proteins examined, with a few exceptions. This strongly suggests that SFN activates signaling pathways that are similar to those induced by exercise and warrants further investigation with an in vivo model of exercise.

SFN treatment also increased the levels of lysosomal-related proteins TFE3, Cathepsin B, and vATPase (72). It is important to note that the relationship between SFN and the lysosome has been significantly underexplored, especially within the content of skeletal muscle. However, two studies have reported that SFN enhanced lysosomal area and lysosomal proteins (73, 74). Furthermore, Nrf-2 overexpression resulted in a marked increase in lysosomal biogenesis, suggesting that Nrf-2 may indeed regulate lysosomal content (75). Interestingly, this may be driven by the ARE site found within the TFE3 promoter region (76), which may mediate the enhancement in lysosome content observed. Together, this suggests that SFN increases cellular degradation capacity, which is useful for enhancing mitochondrial turnover to ensure the quality of the mitochondrial pool.

Although limited literature has examined the role of SFN when coupled with exercise, there is evidence to suggest SFN may support muscle health. Indeed, SFN pretreatment has been reported to blunt exercise-induced muscle damage, evident through a reduction in plasma creatine phosphokinase (CPK) relative to nontreated exercised rats (77). Similar results have been observed in human skeletal muscle, where 4 wk of SFN ingestion reduced CPK release and the proinflammatory cytokine IL-6 following high-intensity exercise (78). However, to our knowledge, there are currently no studies examining the effect of SFN when coupled with chronic exercise. When considering the therapeutic potential of this agent within skeletal muscle research, 12 wk of SFN treatment was reported to enhance mitochondrial respiration, improve grip strength, and time to exhaustion in aged mice (79). Similarly, SFN restored lean muscle mass and grip strength in diabetic mice (80), together suggesting that SFN may hold therapeutic prospects in various models of skeletal muscle dysfunction.

In conclusion, our results indicate that SFN increases lysosomal, mitochondrial, and antioxidant-related proteins similar to our in vitro model of chronic contractile activity. These changes are likely facilitated by Nrf-2, which translocates to the nucleus and enhances the expression of target genes. Although further investigation is required to elucidate the precise mechanisms underlying these pathways, this study demonstrates that SFN can dramatically enhance the mitochondrial phenotype within skeletal muscle cells.

DATA AVAILABILITY

All raw data are available upon request from D.A. Hood (dhood@yorku.ca).

SUPPLEMENTAL MATERIAL

Supplemental Figs. S1 and S2: https://doi.org/10.6084/m9.figshare.27680190.

Supplemental Video S1: https://doi.org/10.6084/m9.figshare.27680046.

GRANTS

This work was supported by Funding from the Natural Sciences and Engineering Research Council of Canada (NSERC; 03623) to D.A. Hood. S. Champsi is a recipient of the Canada Graduate Scholarship-Master's (CGS-M) NSERC Award.

DISCLOSURES

No conflicts of interest, financial or otherwise, are declared by the authors.

AUTHOR CONTRIBUTIONS

S.C. and D.A.H. conceived and designed research; S.C. performed experiments; S.C. analyzed data; S.C. interpreted results of experiments; S.C. prepared figures; S.C. drafted manuscript; S.C. and D.A.H. edited and revised manuscript; S.C. and D.A.H. approved final version of manuscript.

REFERENCES

1. **Hyatt H**, **Deminice R**, **Yoshihara T**, **Powers SK.** Mitochondrial dysfunction induces muscle atrophy during prolonged inactivity: a review of the causes and effects. *Arch Biochem Biophys* 662: 49–60, 2019. doi:10.1016/j.abb.2018.11.005.
2. **Li YP**, **Chen Y**, **John J**, **Moylan J**, **Jin B**, **Mann DL**, **Reid MB.** TNF-α acts via p38 MAPK to stimulate expression of the ubiquitin ligase atrogin1/MAFbx in skeletal muscle. *FASEB J* 19: 362–370, 2005. doi:10.1096/fj.04-2364com.
3. **Glancy B**, **Hartnell LM**, **Malide D**, **Yu ZX**, **Combs CA**, **Connelly PS**, **Subramaniam S**, **Balaban RS.** Mitochondrial reticulum for cellular energy distribution in muscle. *Nature* 523: 617–620, 2015. doi:10.1038/nature14614.
4. **Picard M**, **White K**, **Turnbull DM.** Mitochondrial morphology, topology, and membrane interactions in skeletal muscle: a quantitative three-dimensional electron microscopy study. *J Appl Physiol (1985)* 114: 161–171, 2013. doi:10.1152/japplphysiol.01096.2012.
5. **Memme JM**, **Erlich AT**, **Phukan G**, **Hood DA.** Exercise and mitochondrial health. *J Physiol* 599: 803–817, 2021. doi:10.1113/JP278853.
6. **Anderson S**, **Bankier AT**, **Barrell BG**, **De Bruijn MHL**, **Coulson AR**, **Drouin J**, **Eperon IC**, **Nierlich DP**, **Roe BA**, **Sanger F**, **Schreier PH**, **Smith AJH**, **Staden R**, **Young IG.** Sequence and organization of the human mitochondrial genome. *Nature* 290: 457–465, 1981. doi:10.1038/290457a0.

7. **Calvo SE**, **Clauser KR**, **Mootha VK.** MitoCarta2.0: an updated inventory of mammalian mitochondrial proteins. *Nucleic Acids Res* 44: D1251–D1257, 2016. doi:10.1093/nar/gkv1003.
8. **Lin J**, **Wu H**, **Tarr PT**, **Zhang CY**, **Wu Z**, **Boss O**, **Michael LF**, **Puigserver P**, **Isotani E**, **Olson EN**, **Lowell BB**, **Bassel-Duby R**, **Spiegelman BM.** Transcriptional co-activator PGC-1α drives the formation of slow-twitch muscle fibres. *Nature* 418: 797–801, 2002. doi:10.1038/nature00904.
9. **Wu Z**, **Puigserver P**, **Andersson U**, **Zhang C**, **Adelmant G**, **Mootha V**, **Troy A**, **Cinti S**, **Lowell B**, **Scarpulla RC**, **Spiegelman BM.** Mechanisms controlling mitochondrial biogenesis and respiration through the thermogenic coactivator PGC-1. *Cell* 98: 115–124, 1999. doi:10.1016/S0092-8674(00)80611-X.
10. **Uguccioni G**, **Hood DA.** The importance of PGC-1α in contractile activity-induced mitochondrial adaptations. *Am J Physiol Endocrinol Physiol* 300: E361–E371, 2011. doi:10.1152/ajpendo.00292.2010.
11. **Adhihetty PJ**, **Uguccioni G**, **Leick L**, **Hidalgo J**, **Pilegaard H**, **Hood DA.** The role of PGC-1α on mitochondrial function and apoptotic susceptibility in muscle. *Am J Physiol Cell Physiol* 297: C217–C225, 2009. doi:10.1152/ajpcell.00070.2009.
12. **Leick L**, **Lyngby SS**, **Wojtaszewski JFP**, **Pilegaard H.** PGC-1α is required for training-induced prevention of age-associated decline in mitochondrial enzymes in mouse skeletal muscle. *Exp Gerontol* 45: 336–342, 2010 [Erratum in *Exp Gerontol* 45: 988, 2010]. doi:10.1016/j.exger.2010.01.011.
13. **Lin J**, **Puigserver P**, **Donovan J**, **Tarr P**, **Spiegelman BM.** Peroxisome proliferator-activated receptor γ coactivator 1β (PGC-1β), a novel PGC-1-related transcription coactivator associated with host cell factor. *J Biol Chem* 277: 1645–1648, 2002. doi:10.1074/jbc.C100631200.
14. **Puigserver P**, **Wu Z**, **Park CW**, **Graves R**, **Wright M**, **Spiegelman BM.** A cold-inducible coactivator of nuclear receptors linked to adaptive thermogenesis. *Cell* 92: 829–839, 1998. doi:10.1016/S0092-8674(00)81410-5.
15. **Handschin C**, **Rhee J**, **Lin J**, **Tarr PT**, **Spiegelman BM.** An autoregulatory loop controls peroxisome proliferator-activated receptor γ coactivator 1α expression in muscle. *Proc Natl Acad Sci USA* 100: 7111–7116, 2003. doi:10.1073/pnas.1232352100.
16. **Akimoto T**, **Pohnert SC**, **Li P**, **Zhang M**, **Gumbs C**, **Rosenberg PB**, **Williams RS**, **Yan Z.** Exercise stimulates Pgc-1α transcription in skeletal muscle through activation of the p38 MAPK pathway. *J Biol Chem* 280: 19587–19593, 2005. doi:10.1074/jbc.M408862200.
17. **Puigserver P**, **Rhee J**, **Lin J**, **Wu Z**, **Yoon JC**, **Zhang C-Y**, **Krauss S**, **Mootha VK**, **Lowell BB**, **Spiegelman BM.** Cytokine stimulation of energy expenditure through p38 MAP kinase activation of PPARγ coactivator-1. *Mol Cell* 8: 971–982, 2001. doi:10.1016/S1097-2765(01)00390-2.
18. **Irrcher I**, **Ljubicic V**, **Hood DA.** Interactions between ROS and AMP kinase activity in the regulation of PGC-1α transcription in skeletal muscle cells. *Am J Physiol Cell Physiol* 296: C116–C123, 2009. doi:10.1152/ajpcell.00267.2007.
19. **Jäger S**, **Handschin C**, **St -PJ**, **Spiegelman BM.** AMP-activated protein kinase (AMPK) action in skeletal muscle via direct phosphorylation of PGC-1α. *Proc Natl Acad Sci USA* 104: 12017–12022, 2007. doi:10.1073/pnas.0705070104.
20. **Puigserver P**, **Spiegelman BM.** Peroxisome proliferator-activated receptor-γ coactivator 1α (PGC-1α): transcriptional coactivator and metabolic regulator. *Endocr Rev* 24: 78–90, 2003. doi:10.1210/er.2002-0012.
21. **Larsson N-G**, **Wang J**, **Wilhelmsson H**, **Oldfors A**, **Rustin P**, **Lewandoski M**, **Barsh GS**, **Clayton DA.** Mitochondrial transcription factor A is necessary for mtDNA maintance and embryogenesis in mice. *Nat Genet* 18: 231–236, 1998. doi:10.1038/ng0398-231.
22. **Kelly DP**, **Scarpulla RC.** Transcriptional regulatory circuits controlling mitochondrial biogenesis and function. *Genes Dev* 18: 357–368, 2004. doi:10.1101/gad.1177604.
23. **Moradi N**, **Sanfrancesco VC**, **Champsi S**, **Hood DA.** Regulation of lysosomes in skeletal muscle during exercise, disuse and aging. *Free Radic Biol Med* 225: 323–332, 2024. doi:10.1016/j.freeradbiomed.2024.09.028.
24. **Kim Y**, **Hood DA.** Regulation of the autophagy system during chronic contractile activity-induced muscle adaptations. *Physiol Rep* 5: e13307, 2017. doi:10.14814/phy2.13307.
25. **Kim Y**, **Triolo M**, **Erlich AT**, **Hood DA.** Regulation of autophagic and mitophagic flux during chronic contractile activity-induced muscle adaptations. *Pflugers Arch* 471: 431–440, 2019. doi:10.1007/s00424-018-2225-x.
26. **Oliveira AN**, **Tamura Y**, **Memme JM**, **Hood DA.** Role of TFEB and TFE3 in mediating lysosomal and mitochondrial adaptations to contractile activity in skeletal muscle myotubes. *Mitochondrial Commun* 1: 73–87, 2023. doi:10.1016/j.mitoco.2023.10.001.
27. **Martina JA**, **Diab HI**, **Lishu L**, **Jeong-A L**, **Patange S**, **Raben N**, **Puertollano R.** The nutrient-responsive transcription factor TFE3 promotes autophagy, lysosomal biogenesis, and clearance of cellular debris. *Sci Signal* 7: ra9, 2014., doi:10.1126/scisignal.2004754.
28. **Powers SK**, **Criswell D**, **Lawler J**, **Ji LL**, **Martin D**, **Herb RA**, **Dudley G.** Influence of exercise and fiber type on antioxidant enzyme activity in rat skeletal muscle. *Am J Physiol Regul Integr Comp Physiol* 266: R375–R380, 1994. doi:10.1152/ajpregu.1994.266.2.R375.
29. **Venditti P**, **Meo SD.** Effect of training on antioxidant capacity, tissue damage, and endurance of adult male rats. *Int J Sports Med* 18: 497–502, 1997. doi:10.1055/s-2007-972671.
30. **Venditti P**, **Di Meo S.** Antioxidants, tissue damage, and endurance in trained and untrained young male rats. *Arch Biochem Biophys* 331: 63–68, 1996. doi:10.1006/abbi.1996.0283.
31. **Itoh K**, **Chiba T**, **Takahashi S**, **Ishii T**, **Igarashi K**, **Katoh Y**, **Oyake T**, **Hayashi N**, **Satoh K**, **Hatayama I**, **Yamamoto M**, **Nabeshima Y.** An Nrf2/Small Maf heterodimer mediates the induction of phase II detoxifying enzyme genes through antioxidant response elements. *Biochem Biophys Res Commun* 236: 313–322, 1997. doi:10.1006/bbrc.1997.6943.
32. **Itoh K**, **Wakabayashi N**, **Katoh Y**, **Ishii T**, **Igarashi K**, **Engel JD**, **Yamamoto M.** Keap1 represses nuclear activation of antioxidant responsive elements by Nrf2 through binding to the amino-terminal Neh2 domain. *Genes Dev* 13: 76–86, 1999. doi:10.1101/gad.13.1.76.
33. **Kobayashi A**, **Kang MI**, **Watai Y**, **Tong KI**, **Shibata T**, **Uchida K**, **Yamamoto M.** Oxidative and electrophilic stresses activate Nrf2 through inhibition of ubiquitination activity of Keap1. *Mol Cell Biol* 26: 221–229, 2006. doi:10.1128/MCB.26.1.221-229.2006.
34. **Suzuki T**, **Muramatsu A**, **Saito R**, **Iso T**, **Shibata T**, **Kuwata K**, **Kawaguchi S**, **Iwawaki T**, **Adachi S**, **Suda H**, **Morita M**, **Uchida K**, **Baird L**, **Yamamoto M.** Molecular mechanism of cellular oxidative stress sensing by Keap1. *Cell Rep* 28: 746–758.e4, 2019. doi:10.1016/j.celrep.2019.06.047.
35. **Wang P**, **Li CG**, **Qi Z**, **Cui D**, **Ding S.** Acute exercise stress promotes Ref1/Nrf2 signalling and increases mitochondrial antioxidant activity in skeletal muscle. *Exp Physiol* 101: 410–420, 2016. doi:10.1113/EP085493.
36. **Hu C**, **Eggler AL**, **Mesecar AD**, **Van Breemen RB.** Modification of Keap1 cysteine residues by sulforaphane. *Chem Res Toxicol* 24: 515–521, 2011. doi:10.1021/tx100389r.
37. **Moradi N**, **Champsi S**, **Hood DA.** Sulforaphane, urolithin A, and ZLN005 induce time-dependent alterations in antioxidant capacity, mitophagy, and mitochondrial biogenesis in muscle cells. *Sports Med Health Sci* 7:16–27, 2024. doi:10.1016/j.smhs.2024.03.011.
38. **Zhang Y**, **Talalay P**, **Cho CG**, **Posner GH.** A major inducer of anticarcinogenic protective enzymes from broccoli: isolation and elucidation of structure. *Proc Natl Acad Sci USA* 89: 2399–2403, 1992. doi:10.1073/pnas.89.6.2399.
39. **Horie Y**, **Suzuki T**, **Inoue J**, **Iso T**, **Wells G**, **Moore TW**, **Mizushima T**, **Dinkova-Kostova AT**, **Kasai T**, **Kamei T**, **Koshiba S**, **Yamamoto M.** Molecular basis for the disruption of Keap1–Nrf2 interaction via Hinge & Latch mechanism. *Commun Biol* 4: 576, 2021. doi:10.1038/s42003-021-02100-6.
40. **Yagishita Y**, **Fahey JW**, **Dinkova-Kostova AT**, **Kensler TW.** Broccoli or sulforaphane: is it the source or dose that matters? *Molecules* 24: 3593, 2019. doi:10.3390/molecules24193593.
41. **Castro NP**, **Rangel MC**, **Merchant AS**, **MacKinnon G**, **Cuttitta F**, **Salomon DS**, **Kim YS.** Sulforaphane suppresses the growth of triple-negative breast cancer stem-like cells in vitro and in vivo. *Cancer Prev Res (Phila)* 12: 147–158, 2019. doi:10.1158/1940-6207.CAPR-18-0241.
42. **Piantadosi CA**, **Carraway MS**, **Babiker A**, **Suliman HB.** Heme oxygenase-1 regulates cardiac mitochondrial biogenesis via Nrf2-mediated transcriptional control of nuclear respiratory factor-1. *Circ Res* 103: 1232–1240, 2008. doi:10.1161/01.RES.0000338597.71702.ad.

43. **Crilly MJ**, **Tryon LD**, **Erlich AT**, **Hood DA.** The role of Nrf2 in skeletal muscle contractile and mitochondrial function. *J Appl Physiol (1985)* 121: 730–740, 2016. doi:10.1152/japplphysiol.00042.2016.
44. **Birnbaum JH**, **Wanner D**, **Gietl AF**, **Saake A**, **Kündig TM**, **Hock C**, **Nitsch RM**, **Tackenberg C.** Oxidative stress and altered mitochondrial protein expression in the absence of amyloid-β and tau pathology in iPSC-derived neurons from sporadic Alzheimer's disease patients. *Stem Cell Res* 27: 121–130, 2018. doi:10.1016/j.scr.2018.01.019.
45. **Bhattacharya D**, **Slavin MB**, **Hood DA.** Muscle mitochondrial transplantation can rescue and maintain cellular homeostasis. *Am J Physiol Cell Physiol* 325: C862–C884, 2023. doi:10.1152/ajpcell.00212.2023.
46. **Bolte S**, **Cordelières FP.** A guided tour into subcellular colocalization analysis in light microscopy. *J Microsc* 224: 213–232, 2006. doi:10.1111/j.1365-2818.2006.01706.x.
47. **Chaudhry A**, **Shi R**, **Luciani DS.** A pipeline for multidimensional confocal analysis of mitochondrial morphology, function, and dynamics in pancreatic β-cells. *Am J Physiol Endocrinol Physiol* 318: E87–E101, 2020. doi:10.1152/ajpendo.00457.2019.
48. **Hemel IMGM**, **Engelen BPH**, **Luber N**, **Gerards M.** A hitchhiker's guide to mitochondrial quantification. *Mitochondrion* 59: 216–224, 2021. doi:10.1016/j.mito.2021.06.005.
49. **Memme JM**, **Sanfrancesco VC**, **Hood DA.** Activating transcription factor 4 regulates mitochondrial content, morphology, and function in differentiating skeletal muscle myotubes. *Am J Physiol Cell Physiol* 325: C224–C242, 2023. doi:10.1152/ajpcell.00080.2023.
50. **Connor MK**, **Irrcher I**, **Hood DA.** Contractile activity-induced transcriptional activation of cytochrome c involves Sp1 and is proportional to mitochondrial ATP synthesis in C2C12 muscle cells. *J Biol Chem* 276: 15898–15904, 2001. doi:10.1074/jbc.M100272200.
51. **Koopman WJ**, **Verkaart S**, **Visch HJ**, **Van Emst-de Vries S**, **Nijtmans LG**, **Smeitink JA**, **Willems PH.** Human NADH:ubiquinone oxidoreductase deficiency: Radical changes in mitochondrial morphology? *Am J Physiol Cell Physiol* 293: C22–C29, 2007 [Erratum in *Am J Physiol Cell Physiol* 320: C152–C154, 2021]. doi:10.1152/ajpcell.00194.2006.
52. **Hood DA**, **Memme JM**, **Oliveira AN**, **Triolo M.** Maintenance of skeletal muscle mitochondria in health, exercise, and aging. *Annu Rev Physiol* 81: 19–41, 2019. doi:10.1146/annurev-physiol-020518-114310.
53. **Joo MS**, **Kim WD**, **Lee KY**, **Kim JH**, **Koo JH**, **Kim SG.** AMPK facilitates nuclear accumulation of Nrf2 by phosphorylating at serine 550. *Mol Cell Biol* 36: 1931–1942, 2016. doi:10.1128/MCB.00118-16.
54. **Xu C**, **Yuan X**, **Pan Z**, **Shen G**, **Kim J-H**, **Yu S**, **Khor TO**, **Li W**, **Ma J**, **Kong A-NT.** Mechanism of action of isothiocyanates: the induction of ARE-regulated genes is associated with activation of ERK and JNK and the phosphorylation and nuclear translocation of Nrf2. *Mol Cancer Ther* 5: 1918–1926, 2006. doi:10.1158/1535-7163.MCT-05-0497.
55. **Masuda M**, **Yoshida-Shimizu R**, **Mori Y**, **Ohnishi K**, **Adachi Y**, **Sakai M**, **Kabutoya S**, **Ohminami H**, **Yamanaka-Okumura H**, **Yamamoto H**, **Miyazaki M**, **Taketani Y.** Sulforaphane induces lipophagy through the activation of AMPK-mTOR-ULK1 pathway signaling in adipocytes. *J Nutr Biochem* 106: 109017, 2022. doi:10.1016/j.jnutbio.2022.109017.
56. **Subedi L**, **Lee J**, **Yumnam S**, **Ji E**, **Kim S.** Anti-inflammatory effect of sulforaphane on LPS-activated microglia potentially through JNK/AP-1/NF-κB inhibition and Nrf2/HO-1 activation. *Cells* 8: 194, 2019. doi:10.3390/cells8020194.
57. **Taguchi K**, **Fujikawa N**, **Komatsu M**, **Ishii T**, **Unno M**, **Akaike T**, **Motohashi H**, **Yamamoto M.** Keap1 degradation by autophagy for the maintenance of redox homeostasis. *Proc Natl Acad Sci USA* 109: 13561–13566, 2012. doi:10.1073/pnas.1121572109.
58. **Zhu L**, **He S**, **Huang L**, **Ren D**, **Nie T**, **Tao K**, **Xia L**, **Lu F**, **Mao Z**, **Yang Q.** Chaperone-mediated autophagy degrades Keap1 and promotes Nrf2-mediated antioxidative response. *Aging Cell* 21: e13616, 2022. doi:10.1111/acel.13616.
59. **Jo C**, **Kim S**, **Cho SJ**, **Choi KJ**, **Yun SM**, **Koh YH**, **Johnson GVW**, **Park SI.** Sulforaphane induces autophagy through ERK activation in neuronal cells. *FEBS Lett* 588: 3081–3088, 2014. doi:10.1016/j.febslet.2014.06.036.
60. **Liu J**, **Huang C**, **Liu J**, **Meng C**, **Gu Q**, **Du X**, **Yan M**, **Yu Y**, **Liu F**, **Xia C.** Nrf2 and its dependent autophagy activation cooperatively counteract ferroptosis to alleviate acute liver injury. *Pharmacol Res* 187: 106563, 2023. doi:10.1016/j.phrs.2022.106563.
61. **Komatsu M**, **Kurokawa H**, **Waguri S**, **Taguchi K**, **Kobayashi A**, **Ichimura Y**, **Sou YS**, **Ueno I**, **Sakamoto A**, **Tong KI**, **Kim M**, **Nishito Y**, **Iemura S**, **Natsume T**, **Ueno T**, **Kominami E**, **Motohashi H**, **Tanaka K**, **Yamamoto M.** The selective autophagy substrate p62 activates the stress responsive transcription factor Nrf2 through inactivation of Keap1. *Nat Cell Biol* 12: 213–223, 2010. doi:10.1038/ncb2021.
62. **Jain A**, **Lamark T**, **Sjøttem E**, **Bowitz Larsen K**, **Atesoh Awuh J**, **Øvervatn A**, **McMahon M**, **Hayes JD**, **Johansen T.** p62/SQSTM1 is a target gene for transcription factor NRF2 and creates a positive feedback loop by inducing antioxidant response element-driven gene transcription. *J Biol Chem* 285: 22576–22591, 2010. doi:10.1074/jbc.M110.118976.
63. **Negrette-Guzmán M**, **Huerta-Yepez S**, **Vega MI**, **León-Contreras JC**, **Hernández-Pando R**, **Medina-Campos ON**, **Rodríguez E**, **Tapia E**, **Pedraza-Chaverri J.** Sulforaphane induces differential modulation of mitochondrial biogenesis and dynamics in normal cells and tumor cells. *Food Chem Toxicol* 100: 90–102, 2017. doi:10.1016/j.fct.2016.12.020.
64. **O'Mealey GB**, **Berry WL**, **Plafker SM.** Sulforaphane is a Nrf2-independent inhibitor of mitochondrial fission. *Redox Biol* 11: 103–110, 2017. doi:10.1016/j.redox.2016.11.007.
65. **Scarpulla RC**, **Vega RB**, **Kelly DP.** Transcriptional integration of mitochondrial biogenesis. *Trends Endocrinol Metab* 23: 459–466, 2012. doi:10.1016/j.tem.2012.06.006.
66. **Hull TD**, **Boddu R**, **Guo L**, **Tisher CC**, **Traylor AM**, **Patel B**, **Joseph R**, **Prabhu SD**, **Suliman HB**, **Piantadosi CA**, **Agarwal A**, **George JF.** Heme oxygenase-1 regulates mitochondrial quality control in the heart. *JCI Insight* 1: e85817, 2016. doi:10.1172/jci.insight.85817.
67. **Alves De Souza RW**, **Gallo D**, **Lee GR**, **Katsuyama E**, **Schaufler A**, **Weber J**, **Csizmadia E**, **Tsokos GC**, **Koch LG**, **Britton SL**, **Wisløff U**, **Brum PC**, **Otterbein LE.** Skeletal muscle heme oxygenase-1 activity regulates aerobic capacity. *Cell Rep* 35: 109018, 2021. doi:10.1016/j.celrep.2021.109018.
68. **Salatino S**, **Kupr B**, **Baresic M**, **Omidi S**, **van Nimwegen E**, **Handschin C.** The genomic context and corecruitment of SP1 affect ERRα coactivation by PGC-1α in muscle cells. *Mol Endocrinol* 30: 809–825, 2016 [Erratum in *Endocrinology* 159: 2703, 2018]. doi:10.1210/me.2016-1036.
69. **Herzig S**, **Long F**, **Jhala US**, **Hedrick S**, **Quinn R**, **Bauer A**, **Rudolph D**, **Schutz G**, **Yoon C**, **Puigserver P**, **Spiegelman B**, **Montminy M.** CREB regulates hepatic gluconeogenesis through the coactivator PGC-1. *Nature* 413: 179–183, 2001 [Erratum in *Nature* 413: 652, 2001]. doi:10.1038/35093131.
70. **Adamovich Y**, **Shlomai A**, **Tsvetkov P**, **Umansky KB**, **Reuven N**, **Estall JL**, **Spiegelman BM**, **Shaul Y.** The protein level of PGC-1α, a key metabolic regulator, is controlled by NADH-NQO1. *Mol Cell Biol* 33: 2603–2613, 2013. doi:10.1128/MCB.01672-12.
71. **Asher G**, **Tsvetkov P**, **Kahana C**, **Shaul Y.** A mechanism of ubiquitin-independent proteasomal degradation of the tumor suppressors p53 and p73. *Genes Dev* 19: 316–321, 2005. doi:10.1101/gad.319905.
72. **Triolo M**, **Hood DA.** Mitochondrial breakdown in skeletal muscle and the emerging role of the lysosomes. *Arch Biochem Biophys* 661: 66–73, 2019. doi:10.1016/j.abb.2018.11.004.
73. **Li D**, **Shao R**, **Wang N**, **Zhou N**, **Du K**, **Shi J**, **Wang Y**, **Zhao Z**, **Ye X**, **Zhang X**, **Xu H.** Sulforaphane activates a lysosome-dependent transcriptional program to mitigate oxidative stress. *Autophagy* 17: 872–887, 2021. doi:10.1080/15548627.2020.1739442.
74. **Ye X**, **Toyama T**, **Taguchi K**, **Arisawa K**, **Kaneko T**, **Tsutsumi R**, **Yamamoto M**, **Saito Y.** Sulforaphane decreases serum selenoprotein P levels through enhancement of lysosomal degradation independent of Nrf2. *Commun Biol* 6: 1060, 2023. doi:10.1038/s42003-023-05449-y.
75. **Ong AJS**, **Bladen CE**, **Tigani TA**, **Karamalakis AP**, **Evason KJ**, **Brown KK**, **Cox AG.** The KEAP1–NRF2 pathway regulates TFEB/TFE3-dependent lysosomal biogenesis. *Proc Natl Acad Sci USA* 120: e2217425120, 2023. doi:10.1073/pnas.2217425120.
76. **Chorley BN**, **Campbell MR**, **Wang X**, **Karaca M**, **Sambandan D**, **Bangura F**, **Xue P**, **Pi J**, **Kleeberger SR**, **Bell DA.** Identification of novel NRF2-regulated genes by ChIP-Seq: influence on retinoid X receptor alpha. *Nucleic Acids Res* 40: 7416–7429, 2012. doi:10.1093/nar/gks409.
77. **Malaguti M**, **Angeloni C**, **Garatachea N**, **Baldini M**, **Leoncini E**, **Collado PS**, **Teti G**, **Falconi M**, **Gonzalez-Gallego J**, **Hrelia S.** Sulforaphane treatment protects skeletal muscle against damage induced by exhaustive exercise in rats. *J Appl Physiol (1985)* 107: 1028–1036, 2009. doi:10.1152/japplphysiol.00293.2009.

78. **Sato K**, **Kihara H**, **Kumazawa Y**, **Tatara K.** Oral chronic sulforaphane effects on heavy resistance exercise: Implications for inflammatory and muscle damage parameters in young practitioners. *Nutrition* 90: 111266, 2021. doi:10.1016/j.nut.2021.111266.
79. **Bose C**, **Alves I**, **Singh P**, **Palade PT**, **Carvalho E**, **Børsheim E**, **Jun S**, **Cheema A**, **Boerma M**, **Awasthi S**, **Singh SP.** Sulforaphane prevents age-associated cardiac and muscular dysfunction through Nrf2 signaling. *Aging Cell* 19: e13261, 2020. doi:10.1111/acel.13261.
80. **Wang M**, **Pu D**, **Zhao Y**, **Chen J**, **Zhu S**, **Lu A**, **Liao Z**, **Sun Y**, **Xiao Q.** Sulforaphane protects against skeletal muscle dysfunction in spontaneous type 2 diabetic db/db mice. *Life Sci* 255: 117823, 2020. doi:10.1016/j.lfs.2020.117823.